



VILNIUS UNIVERSITY
FACULTY OF CHEMISTRY AND GEOSCIENCES
INSTITUTE OF CHEMISTRY
DEPARTMENT OF INORGANIC CHEMISTRY

Rūta Gerulaitytė

Pharmaceutical chemistry

Master thesis

**PERYLENE DYES AT NATURAL FLUORESCENT MINERALS: ROUTE TOWARDS
HYDRID MATERIALS VIA ONE POT HYDROTHERMAL SYNTHESIS**

Scientific adviser

prof. dr. Aivaras Kareiva

(permission to defend, date, signature)

Date of submission _____

Registration No. _____

Vilnius 2020

TABLE OF CONTENTS

ABBREVIATIONS	4
INTRODUCTION	5
1. LITERATURE.....	7
1.1 Minerals	7
1.2 Hydrothermal synthesis	7
1.3 Fluorescent minerals.....	8
1.4 Silicates.....	9
1.5 Phyllosilicates	10
1.6 Gyrolite.....	11
1.7 Ni-Hectorite	12
1.8 Zn-Phlogopite	13
1.9 Perylene dye	14
2. EXPERIMENTAL SECTION.....	15
2.1 Materials	15
2.2 Synthesis of Gyrolite	15
2.3 Synthesis of Ni-Hectorite	16
2.4 Synthesis of Ni-Phyllosilicates.....	16
2.4.1 Synthesis of 1:1 Ni-Phyllosilicates.....	16
2.4.2 Synthesis of 2:1 Ni-Phyllosilicates.....	17
2.4.3 Synthesis of Aminopropyl-Ni-Phyllosilicates and PBI@Ni-Phyllosilicates.....	18
2.5 Hydrothermal synthesis of Zn-Phlogopite and PBI@Zn-Phlogopite.....	19
2.6 Characterization.....	20
3. RESULTS AND DISCUSSION.....	22
3.1 Gyrolite.....	22
3.2 Ni-Hectorite	23
3.3 Ni-Phyllosilicates.....	23
3.4 Aminopropyl-modified 2:1 Ni-Phyllosilicates and PBI@Ni-Phyllosilicates.....	24
3.4.1 The crystallinity of aminopropyl-modified Ni-Phyllosilicates and their hybrid materials by PXRD.....	25
3.4.2 The local order of aminopropyl-modified Ni-Phyllosilicates and their hybrid materials by ATR-FTIR	26
3.4.3 UV measurements.....	28

3.4.4	Fluorescence	30
3.4.5	Morphology of aminopropyl-modified Ni-Phyllosilicates and their hybrid materials..	31
3.5	Zn-Phlogopite and PBI@Zn-Phlogopite	31
3.5.1	The crystallinity of Zn-Phlogopite and their hybrid materials by PXRD.....	32
3.5.2	The local order of Zinc phlogopite and their hybrid materials by ATR-FTIR.....	34
3.5.3	UV measurements.....	36
3.5.4	Fluorescence`	38
3.5.5	Morphology of Zn-Phlogopites and their hybrid materials	39
4.	CONCLUSION AND OUTLOOK	40
5.	REFERENCES	41
	SUMMARY.....	45
	SANTRAUKA.....	46
	ACKNOWLEDGEMENTS.....	47

ABBREVIATIONS

APTS – (3-Aminopropyl) triethoxysilane

ATR-FTIR – Attenuated Total Reflectance Fourier Transform InfraRed

HT – Hydrothermal

NBI – Naphthalene bisimide

PBA – Perylene-3,4,9,10-tetracarboxylic dianhydride

PBI – Perylene bisimide

PXRD – Powder X-Ray Diffraction

SEM – Scanning Electron Microscopy

TEOS – Tetraethyl orthosilicate

UV-Vis – Ultraviolet-Visible spectroscopy

INTRODUCTION

Fluorescent minerals are minerals that when exposed to ultraviolet radiation they emit visible light. Fluorescence happens when invisible short wavelength radiation is absorbed by a material and then it is converted and re-emitted as a longer wavelength (Fish & Agoston, 1980). Most fluorescent minerals require an activator to initiate fluorescence. Fluorescence can also be caused by crystal structure defects or organic impurities. Activators are responsible for the types of fluorescence. A mineral may fluoresce with different colors or brightnesses when exposed to different activators. Some may produce bright and vibrant colors while others are barely visible.

Usually, minerals that are not naturally fluorescent can become fluorescent by the addition of organic chromophores. One example is laponite clay mineral and two organic dyes: Fluorescein and Rhodamine 6G (Saha et al., 2015).

Phyllosilicates are attractive minerals due to their layered characteristics, which display interesting adsorptive and ion-exchange properties, thermal and chemical stability. Recently, phyllosilicates composites have attracted attention for their possible uses in drug delivery systems (Shunmugasamy et al., 2015). Clay composites have been studied for their ability to control drug delivery in order to improve effectiveness and reduce side effects (Gârea et al., 2017). Moreover, clays can be prepared in the laboratory by hydrothermal synthesis (HTS) and have their surface modified by organic groups. Some studies report the use of an organic group bound to the Si atom of a trialkoxyalkylsilane reactant in order to make them more prone to reactions in the interlayer space (Ferreira et al., 2008).

In this work, we are interested on aminopropyl-modified minerals (Fig. 1A). The $-NH_2$ groups are important for the formation of bisimides dyes, in particular, perylene bisimide dyes (PBI), generating an interesting hybrid material (Fig. 1B).

Perylene derivatives are high performance pigments, and they are interesting due to their intense visible light absorption, high thermal and chemical stability, electron accepting ability, and unique quantum yields in solution (Türkmen et al., 2009). However, their synthesis (Fig. 1C) includes the use of harmful and toxic solvents as dicyclohexylcarbodiimide or dimethylformamide (DMF). The method used by Langhals, generate high efficiency of NBIs and PBIs, the products must be chromatographically purified or recrystallized (Langhals, 1985). In addition, typically 4-fold (in some cases up to 20-fold) molar excess of the monoamines is used which is highly unwanted in terms of “green chemistry”. (Baumgartner et al., 2017)

Recently, UnterlassLab (Baumgartner et al., 2017) has shown that PBIs can be obtained under hydrothermal conditions, which is inherently a green approach. Hydrothermal synthesis (HTS) consists of pressure, temperature, water, and autoclave.

Since both layered minerals and PBIs can be obtained under HT conditions, the combination of both components, generating a hybrid material by one-pot green method, might be reachable. Thus, in this work we aimed the preparation and characterization of four different fluorescent minerals together with the synthesis of PBI by one-pot hydrothermal synthesis. The minerals were chosen by their properties illustrated in Fig. 2.

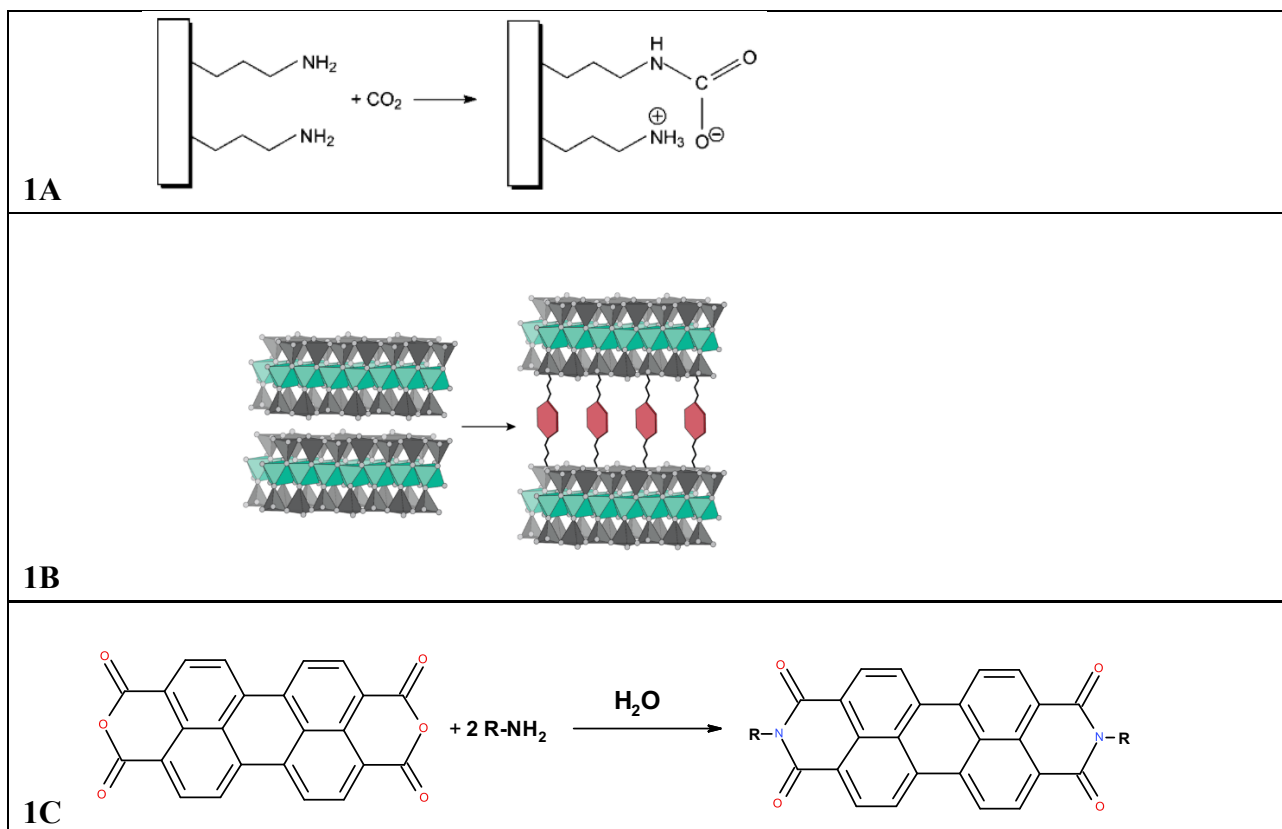


Figure 1. A) Aminopropyl – modified mineral (Ferreira et al., 2008); b) clay and perylene bisimide dye hybrid material; c) reaction between PBA and an amine (Baumgartner et al., 2017).





 <p style="text-align: center;">Gyrolite</p>	 <p style="text-align: center;">Hectorite</p>	 <p style="text-align: center;">Phyllosilicate (Talc)</p>	 <p style="text-align: center;">Phlogopite</p>
<p>$\text{NaCa}_{16}\text{O}_{60}(\text{OH})_8 \cdot 14\text{H}_2\text{O}$ Chemical Class: PHYLLOSILICATES Fluorescent: Short UV=white, Long UV=white.</p>	<p>$\text{Na}_{0.3}(\text{Mg},\text{Li})_3\text{Si}_4\text{O}_{10}(\text{O},\text{H})_2$ Chemical Class: PHYLLOSILICATES Fluorescent, Short UV=weak sky blue, Long UV=bright sky blue.</p>	<p>Tetrahedral and octahedral layers combined in the ratio of 1:1 or 2:1 Fluorescence – depends on a mineral.</p>	<p>$\text{KMg}_3(\text{Si}_3\text{Al})\text{O}_{10}(\text{F},\text{O},\text{H})_2$ Chemical Class: PHYLLOSILICATE S Fluorescent, Short UV=Straw to Lemon Yellow.</p>

Figure 2. Natural minerals and their properties.

1. LITERATURE

1.1 Minerals

A mineral is a homogeneous solid chemical compound with a distinctive chemical composition and a highly ordered atomic arrangement that occurs naturally. Typically it is formed by inorganic processes (Cilek, 2009). Minerals are usually associated with rocks due to the presence of minerals within rocks (Peterson et al., 1996).

A mineral which, by definition, must be formed by natural processes is different from the synthetic equivalents produced by the laboratory. Artificial mineral forms are often developed in manufacturing and research facilities and are most nearly identical to their natural counterparts (Gaft et al., 2015).

Minerals are categorized by variety, species, series, and group in order to maximize their generality. The basic classification level is that of mineral species, each of which is distinguished from the other by its specific chemical and physical properties. All minerals belong to a chemical group, representing their specific components or compounds. Sulfides, oxides, halides, carbonates, nitrates, borates, sulfates, chromates, phosphates, arsenates, vanadates, tungstates, molybdates, and silicates are known as classified chemical groups. Silicate minerals form around 83,3% of the Earth's mantle. (Bleam, 2017)

Minerals form in all geologic environments, under a lot of different chemical and physical conditions, such as temperature and pressure. The major categories of minerals formation are: 1. igneous, or magmatic, in which minerals crystallize from a melt; 2. sedimentary, a raw materials are particles from other rocks that went through weathering or erosion; 3. metamorphic, in which new minerals form at the expense of earlier ones owing to the effects of changing – usually increasing – temperature or pressure or both on some existing rock type; 4. hydrothermal, in which minerals are chemically precipitated from hot solutions within Earth.

1.2 Hydrothermal synthesis

Hydrothermal synthesis refers to heterogeneous reactions in aqueous media above 100 °C and 1bar. Excellent examples of hydrothermal reactions are supplied by nature. Numerous minerals have been formed under these circumstances, and geologists and mineralogists have been able to determine the conditions necessary for mineral formation. In industry, hydrothermal processes play a role in the concepts of hydrometallurgy, e.g., the classic Bayer process for the decomposition of bauxite. This short summary concentrates on the use of hydrothermal chemistry in materials synthesis. A much fuller account of use of the hydrothermal synthesis in preparative chemistry has been given by (Rabenau, 1985).

The term, hydrothermal, comes from geology. In the 19th century geology scientist started to simulate hydrothermal conditions to study the formation of certain minerals. During the industrial revolution equipment and techniques were greatly improved which led scientist to apply hydrothermal methods to single crystal growth. The hydrothermal method refers to the use of an aqueous solution in a special closed reaction vessel (Figure 3a) as a reaction system to create a high-temperature and high-pressure reaction environment by heating and pressurizing the reaction system

(or the vapor pressure produce by itself). The process dissolves and recrystallizes an insoluble or poorly soluble material under normal conditions. The general hydrothermal method preparation steps are shown in Figure 3b.

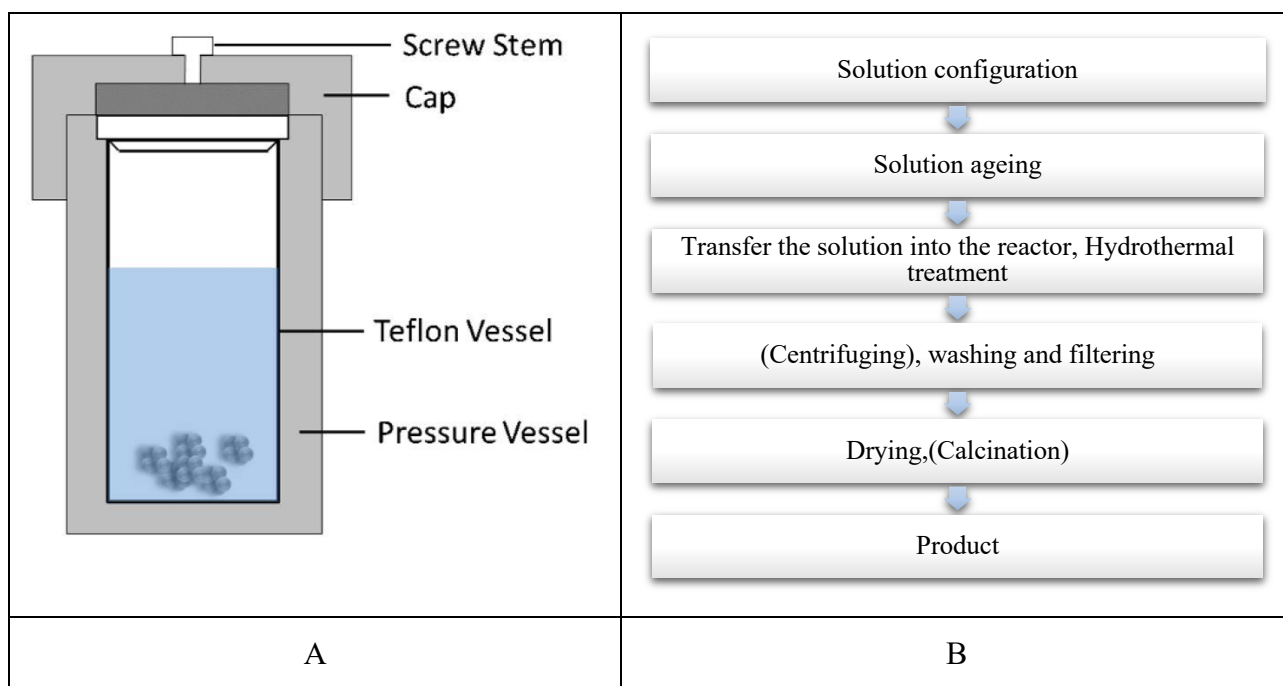


Figure 3. A) Hydrothermal method reaction system (Yang & Park, 2019); b) general steps for hydrothermal preparation.

1.3 Fluorescent minerals

Fluorescence is a form of luminescence in which the light of a certain wavelength irradiates a substance and, as a result, emits longer wavelength light (Valeur & Berberan-Santos, 2011). Ultraviolet lamp light reacts with a mineral's chemicals and causes the mineral to glow (Modreski & Aumente-Modreski, 1996). Photon absorption leads to near-immediate reemission of photons with a longer wavelength. This emission ends almost instantly after turning off the exciting radiation. When activated by invisible ultraviolet light (UV), X-rays and/or electron beams, the fluorescent minerals emit visible light (Mukherjee, 2011).

In general, fluorescence in minerals occurs under two UV wavelengths: short wavelength (SW) and long wavelength (LW) (Bostwick, 1992). SW lamps produce UV radiation at 253.7 nm, LW lamp radiation has two different wavelengths, one peak is at about 351 nm (known as LW350) and another is at about 368 nm (known as LW370) (Newsome, 1998). Many minerals fluoresce under short wavelength and/or one of the long wavelengths, but not both LW. Minerals which are fluorescent under both wavelengths, normally in the same color, but there are some which fluoresce brighter under short wavelength (Bostwick, 1992).

The majority of natural fluorescent minerals are not fluorescent when pure. In order to make the mineral fluoresce, a certain amount of impurities is required. These impurities are called "activators". Different activators can make the same mineral fluoresce in various colors (Borovik, 1989). Various minerals require different activators and different quantities of it (Mukherjee, 2011).

There are some minerals that fluoresce when they are pure. Those include scheelite, powellite and other uranium minerals, known as "self-activated" minerals (Borovik, 1989). Other suspected self-activations include benitoite, cerussite, anglesite, and possibly many other lead minerals (Mukherjee, 2011).

Displaced or incomplete atoms in crystal structure can make defects which are disturbing the electromagnetic balance between the atoms and their vicinity and that could lead to minerals becoming fluorescent (Mukherjee, 2011).

1.4 Silicates

Silicate minerals are rock forming minerals consisting groups of silicate. With a few exceptions all rock-forming minerals are silicates, and they thus constitute more than 83,3% of Earth's crust. (Taylor S.R, 1964)

As one of the biggest groups of minerals, silicates groups, their silicate anions and mineral groups are shown in figure 4 A, and in figure 4 B polymeric silicate anions of the six major silicate mineral groups.

A	Silicate Group	Silicate Anion	Mineral Group
	Nesosilicates	SiO_4^{4-}	Olivine
	Sorosilicates	$\text{Si}_2\text{O}_7^{6-}$	Epidote
	Cyclosilicates	$\text{Si}_3\text{O}_9^{6-}$	Cyclo wollastonite
	Cyclosilicates	$\text{Si}_6\text{O}_{18}^{12-}$	Beryl group
	Insosilicate	$\text{Si}_2\text{O}_6^{4-}$	Pyroxene
	Insosilicate	$\text{Si}_4\text{O}_{11}^{6-}$	Amphibole
	Phyllosilicate	$\text{AlSi}_3\text{O}_{10}^{3-}$	Mica group
	Phyllosilicate	$\text{Si}_4\text{O}_{10}^{4-}$	Kaolinite group
	Tectosilicate	SiO_2^0	Quartz
	Tectosilicate	$\text{AlSi}_3\text{O}_8^{1-}$	Alkali feldspars
	Tectosilicate	$\text{Al}_2\text{Si}_2\text{O}_8^{2-}$	Plagioclase feldspar

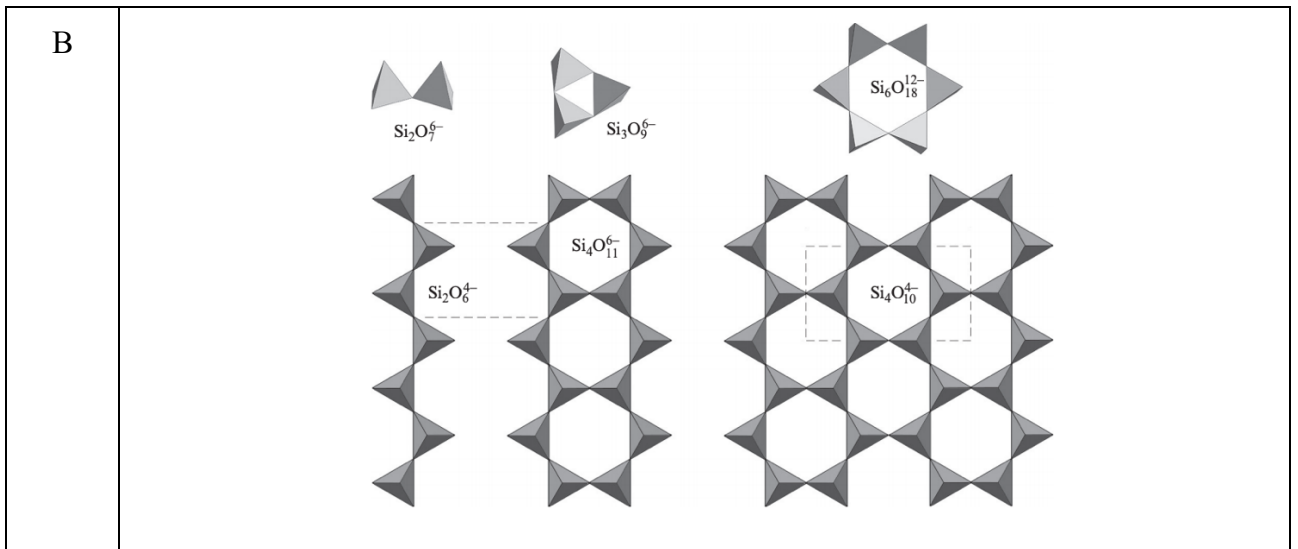


Figure 4. A) Silicate minerals groups; b) polymeric silicate anions of the six major silicate mineral groups. (Bleam, 2017)

1.5 Phyllosilicates

The phyllosilicates, or sheet silicates, are an important group of minerals, that includes the micas, chlorite, serpentine, talc, and the clay minerals.

The tetrahedral bond structure of carbon-based compounds relies on direct carbon bonds, while oxygen-rich silicate minerals base their tetrahedral geometry on the SiO_4^{-4} silicate tetrahedron and its polymerizing inclination. (Nelson, 2015)

The majority of phyllosilicates contain hydroxyl ion, OH^- , with the OH at the center of the 6 member rings. The group transforms into $\text{Si}_2\text{O}_5(\text{OH})^{-3}$. When other cations are attached to the SiO_4 sheets, they share apical oxygen and ions that bind in the octahedral coordination with the other cations. (Nelson, 2015) (Brigatti et al., 2013)

Phyllosilicates groups are based on structure. There are two kind of layers within the sheet: a) T layers tetrahedral sites – tetrahedral coordination of Si and Al; b) O layers – octahedral sites, mostly Al and Mg, occasionally Fe. T and O layers bounded to form sheet and the space between sheets can be either vacant or filled with interlayer cations, water, or other sheets.

The various stacking arrangements and cation types of tetrahedral sheets and octahedral sheets allow the variety of phyllosilicates in nature to occur.

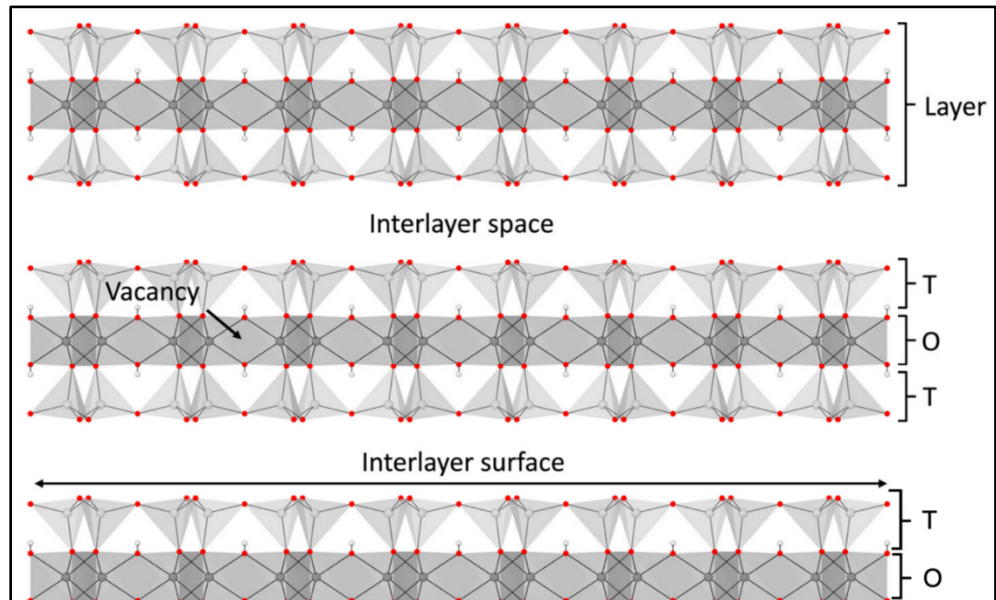
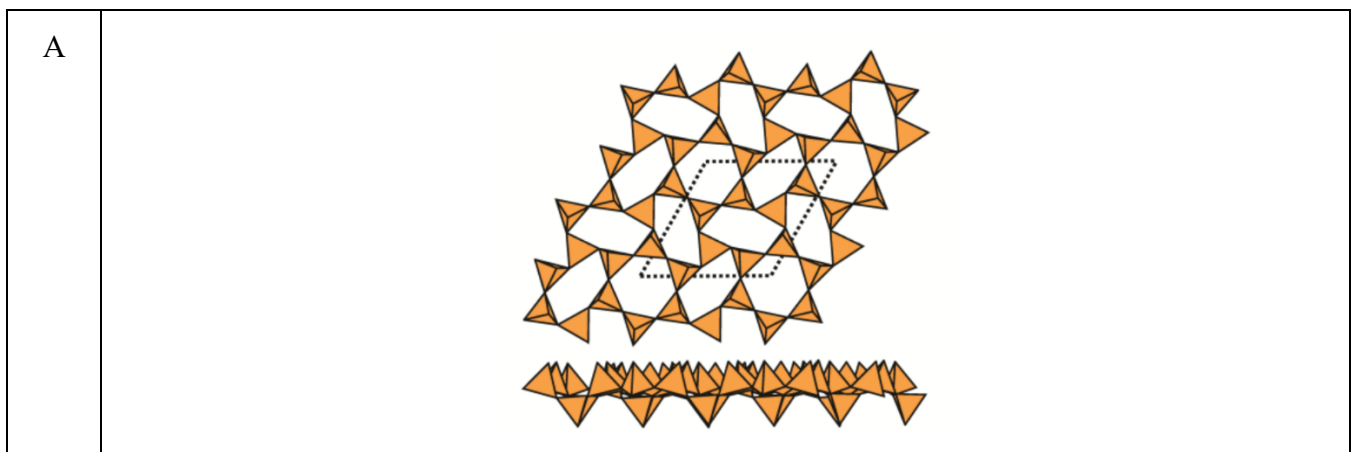


Figure 5. The structure of 2:1 phyllosilicate; T-O-T and T-O layers. (Lavikainen, 2016)

1.6 Gyrolite

Gyrolite, a calcium silicate hydrate, is a phyllosilicate which contains planar sheets (figure 5). It rarely occurs as a natural mineral and is hydrothermally altered basalt and basaltic tuffs (Siauciunas & Baltakys, 2004). First time gyrolite was found on the Isle of Skye, United Kingdom in 1851 by T. Andersen and first time hydrothermally synthesized in 1938 (Flint et al., 1938)(Siauciunas & Baltakys, 2004). The crystal-chemical formula which accounts for most gyrolite samples is $\text{Ca}_{16}\text{Si}_{24}\text{O}_{60}(\text{OH})_8 \cdot (14+x)\text{H}_2\text{O}$, with $0 < x < 3$.

Gyrolite, as a fluorescent mineral, shows it under all wavelengths of ultraviolet light; on short and long wavelengths it glows white (figure 6) (DeMent, 2014).



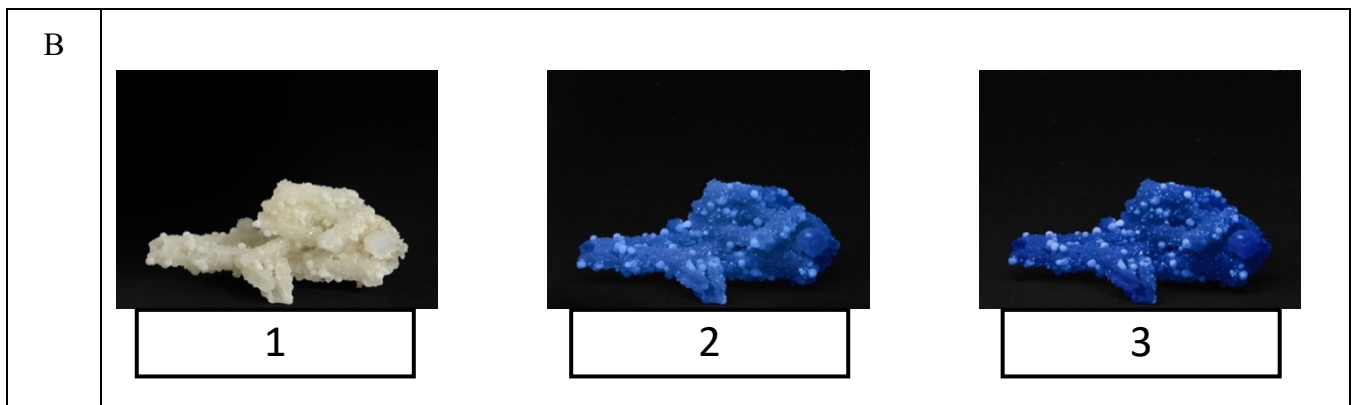


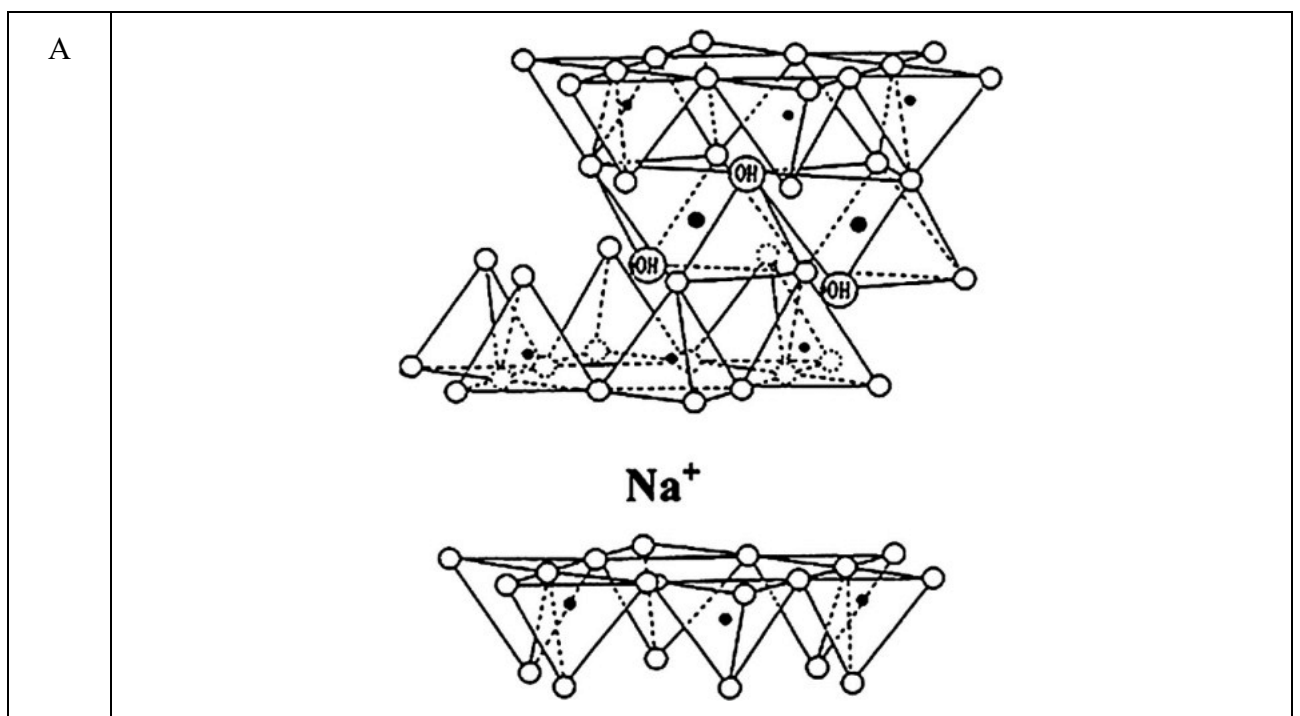
Figure 6. A) Gyrolite planar sheet structure (Hawthorne et al., 2019); b) Gyrolite (round dots) under different lights: 1) natural light; 2) short UV wavelength; 3) long UV wavelength (*Gyrolite - Collection Arkane, n.d.*).

1.7 Ni-Hectorite

Hectorite is a clay mineral from altered volcanic tuff ash with a high silica content related to hot spring activity. Smectite group mineral which is often found together with another phyllosilicate – bentonite. Hectorites ideal chemical formula is $\text{Na}_{0.6}(\text{Mg}_{5.4}, \text{Li}_{0.6})\text{Si}_8\text{O}_{20}(\text{OH})_4 \cdot n\text{H}_2\text{O}$ (Zhang et al., 2019) (NAKAKUKI et al., 2005). Mineral structure is shown in figure 7.

Hectorites fluoresce at short wavelength (254nm) and long wavelength (365nm). At SW it is bluish white (figure 7) and at LW370 – blue.

In this work instead of regular hectorite, which contains magnesium was synthesized nickel hectorite. The whole synthesis was firstly applied by NAKATUKI et al., 2005.



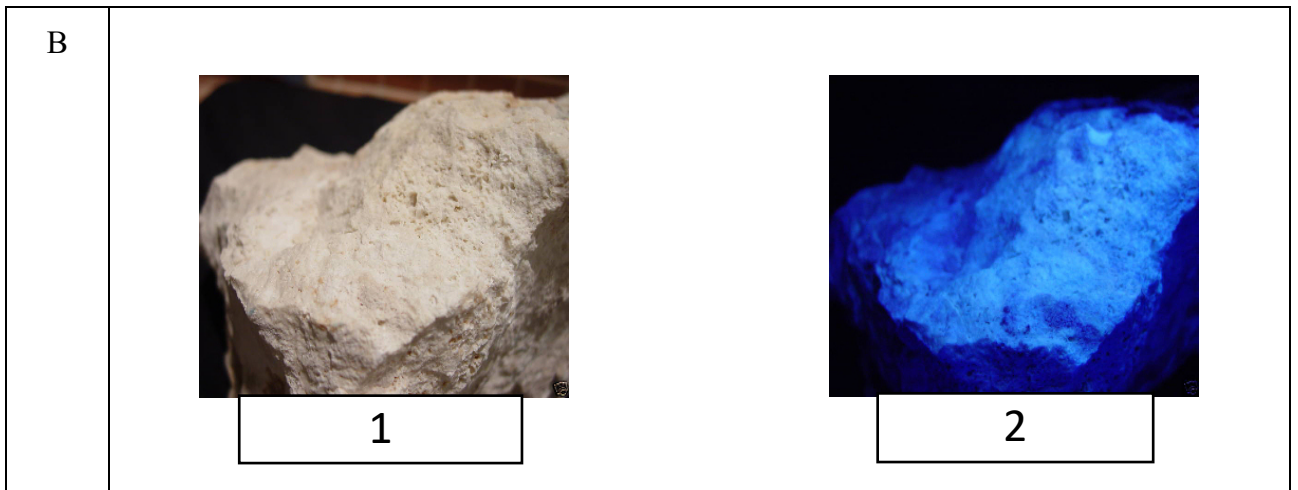


Figure 7. A) Structure of Hectorite (Valapa et al., 2017); Hectorite under: 1) daylight; 2) short UV wavelength (254nm) (Brady, 2010)

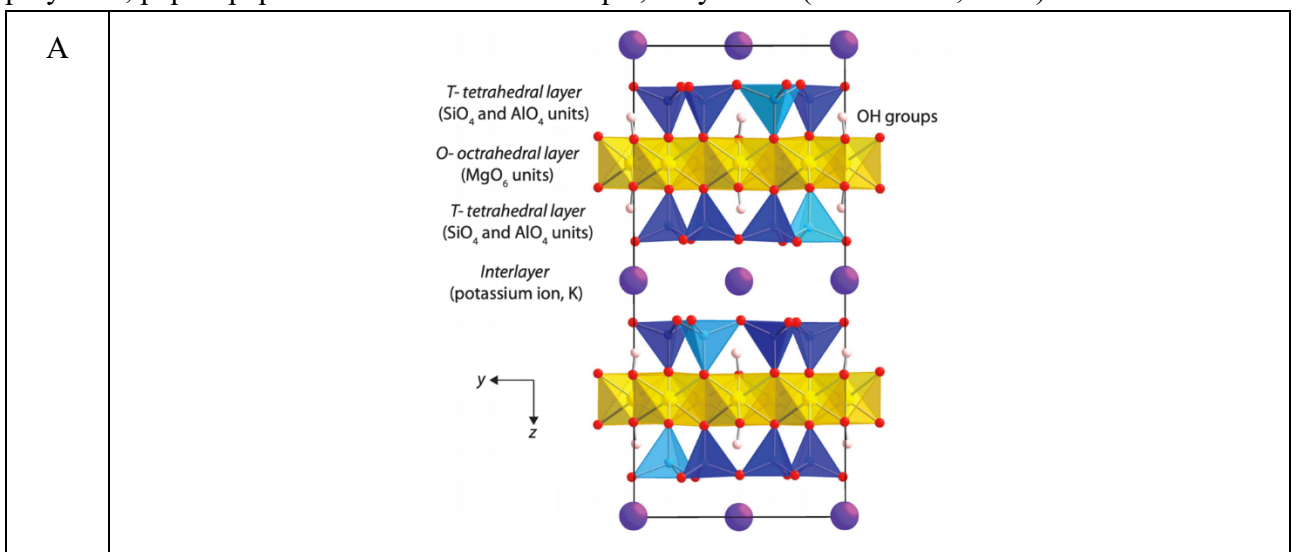
1.8 Zn-Phlogopite

Phlogopite is a mica group phyllosilicate. This mineral's chemical formula $\text{KMg}_3\text{Si}_3\text{AlO}_{10}(\text{F}; \text{OH})_2$. It had tri-octahedral crystal structure, which is shown in figure 8 (Zussman, 1979).

Phlogopite is a fluorescent mineral which under a short UV wavelength lights up from straw to lemon yellow (Bostwick, 1992).

Instead of Magnesium, which contains in original phlogopite, was synthesized Zinc phlogopite ($\text{KZn}_3\text{Si}_3\text{AlO}_{10}(\text{F}; \text{OH})_2$) (Mcguire et al., 2014).

Phlogopite is widely used as: filler, extender, reinforcing agent for adhesives, plastics, rubber, coatings, cosmetics, pearlescent pigments, glass, ceramics, roofing; binder, reinforcement in lipsticks; colorant for external pharmaceuticals, eye use; electrical insulation; asphalt shingles; prod. of vacuum tube spacers; dusting agent lubricant mold release agent; specialty papers for insulation and filtration; wallpaper/wallboard joint cement, oil-well drilling muds; film reinforcing agent, flexibilizer, incandescent lamps, opacifier, filler, slip agent for foods; colorant in food-contact polymers, paper/ paperboard in contact with aqua, fatty foods.(Ash & Ash, 2007)



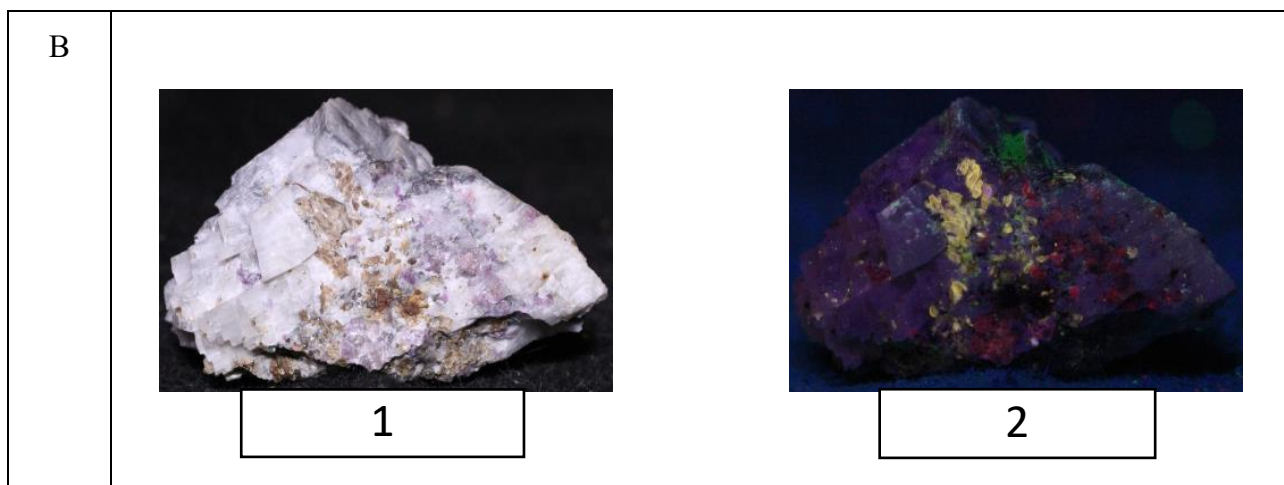


Figure 8. A) Crystal structure of phlogopite (Chheda et al., 2014); b) Phlogopite mica (tan) under: a) daylight; b) short UV wavelength (yellow parts).(Photos by WP).

1.9 Perylene dye

Perylene bisimides (PBIs) and their related derivatives have attracted considerable attention due to their potential applications to the bioimaging and biolabeling sectors.

PBI were initially used exclusively as industrial pigments; they constitute a group of high-performance pigments with red to black shades, depending on the fine details of chemical structure and on molecular packing in the solid state. These pigments exhibit excellent chemical, thermal, photo, and weather stability. This unique chromophore is one of the typical organic semiconductors of the n-type, with high fluorescence and photostability properties.(Rostami-Tapeh-Esmail et al., 2020)(Al-Khateeb et al., 2020)

Due to its high fluorescence, high light tolerance and simple alteration, perylene derivatives have been one of the desirable molecules for biological applications. Scientists try concentrate on applying this genius compound to the bioimaging and biolabeling sectors. (Rostami-Tapeh-Esmail et al., 2020)

Perylene dye connects to the amino group (Fig. 1c) on a modified silica mineral and then incorporates between the layers of chosen mineral (Fig. 1b).

2. EXPERIMENTAL SECTION

2.1 Materials

Zinc sulfate heptahydrate ($\text{ZnSO}_4 \cdot 7\text{H}_2\text{O}$; 99,5%; Sigma-Aldrich), Potassium hydroxide (KOH, $\geq 85\%$, Sigma-Aldrich), Ludox HS-30 colloidal silica (30 wt. % suspension in water, Sigma-Aldrich), (3-Aminopropyl) triethoxysilane (APTS; $\geq 98\%$; Fluka), Tetraethyl orthosilicate (TEOS; $\geq 99.0\%$; Sigma-Aldrich), Perylene-3,4,9,10-tetracarboxylic dianhydride (PBA; 97%; Sigma-Aldrich), Aluminum nitrate nonahydrate ($\text{Al}(\text{NO}_3)_3 \cdot 9\text{H}_2\text{O}$; from university), Nickel (II) nitrate hexahydrate ($\text{Ni}(\text{NO}_3)_2 \cdot 6\text{H}_2\text{O}$; $\geq 98\%$; Merck), Sodium hydroxide (NaOH; $\geq 98\%$; PanReac AppliChem), Calcium hydroxide ($\text{Ca}(\text{OH})_2$; from university), Ethanol (95%; University), Lithium fluoride (LiF; $\geq 99.99\%$; Merck), Nickel (II) chloride hexahydrate ($\text{NiCl}_2 \cdot 6\text{H}_2\text{O}$; $\geq 98.0\%$; Merck), Hydrochloric acid (HCl; $\geq 35\%$; Sigma-Aldrich) and Sodium metasilicate nonahydrate ($\text{Na}_2\text{O}_3\text{Si} \cdot 9\text{H}_2\text{O}$; $\geq 98\%$; Sigma-Aldrich) were used as received.

Sodium orthosilicate was synthesized by wet chemical method, accordingly to reference (Mizutani et al., 1990). In a typical procedure, 36,45 g of sodium metasilicate nonahydrate (0,13 mol) and 10,39 g of sodium hydroxide were dissolved in 100 ml of distilled water to obtain Na_2SiO_3 : NaOH molar ratio of 1: 2. The solution was stirred at 100 °C until the water was evaporated. The powder was calcinated at 600°C for 1h under air.

The solution of silicic acid was prepared by dissolving 2,0712g of sodium orthosilicate in 200 ml of distilled water. The pH of solution was adjusted to 3 with the addition of 3 ml of HCl (2mol/L) and 0,4 ml of concentrated HCl (Mizutani et al., 1990)

Acidic water glass was prepared according to reference (Feng et al., 2018)), by dissolving 142 g sodium metasilicate nonahydrate (0,49 mol) in 100ml water (5,55 mol). The initial pH was 14. To this solution, 15,90 mol of HCl 1 M was added until pH was 3. The solution became a white gel which was filtrated and the solid was dried in an oven for 24h at 80°C.

2.2 Synthesis of Gyrolite

In a typical procedure, 0,88 g of $\text{Ca}(\text{OH})_2$ (11,87 mmol), 24 ml of water and silica source were stirred for 15 minutes at room temperature. Then, the suspension was transferred to PTFE-lined vessel in a stainless-steel autoclave. The autoclave was submitted to hydrothermal treatment for 24 h at 200°C. The crystallization was investigated for 20h, 40h, 48h, 65h and 72h. The autoclaves were cooled down with cold tap water. The products were collected by filtration and washed with distilled water till pH ~ 7 . The solids were rinsed with ethanol and then dried overnight under vacuum at 80°C. After drying, samples were ground till powder. Table 1 shows the composition of the gels for the synthesis of gyrolite.

Table 1. Compositions of the gels for the synthesis of gyrolite.

Sample name	Ca(OH) ₂ [g]	H ₂ O [ml]	Ludox HS-30 [ml]	APTS [ml]	TEOS [ml]	Reaction time [h]
RG-001A	0,8812	24	3	-	-	24
RG-001B	0,8820	24	3	-	-	41
RG-001C	0,8811	24	3	-	-	48
RG-001D	0,8824	24	3	-	-	65
RG-001E	0,8798	24	3	-	-	72
RG-001F	0,8814	24	3	-	-	30
RG-001G	0,4421	12	-	-	6,698	24
RG-001H	0,4413	12	0,74	3,51	-	24
RG-001I	0,4400	12	-	3,51	3,350	24

2.3 Synthesis of Ni-Hectorite

The synthesis of Ni-Hectorite were performed according to reference (NAKAKUKI et al., 2005). In a typical procedure, 2,79 g of nickel (II) chloride hexahydrate (11,73 mmol) was added to 4,13 g of acidic water glass. To the suspension, 0,361 g of NaOH (9 mmol) were added, stirred for 15 minutes, and washed with distilled water. The obtained solid was added to a solution containing NaOH (9 mmol) and LiF (11,95 mmol), yielding a gel of molar composition 0,7 Na₂O: 5,4 NiO: 0,6 Li₂O: 8 SiO₂. Then, the gel was transferred to a PTFE-lined vessel in a stainless-steel autoclave. The autoclave was submitted to hydrothermal treatment for 24h at 200°C. The autoclave was cooled with cold tap water. The solids were collected by centrifugation and washed with distilled water. The solids were dried overnight under vacuum at 80°C. After drying, samples were ground till powder.

2.4 Synthesis of Ni-Phyllosilicates

2.4.1 Synthesis of 1:1 Ni-Phyllosilicates

In a typical synthesis, 1,6050 g of NiCl₂ · 6H₂O was dissolved in 100 ml of an aqueous solution of silicic acid (prepared as described in section 2.1). To this solution, 20,25 ml of NaOH (1 mol/L)

was dropwise and stirred magnetically for 10 min at room temperature. Then, 28 ml of the final gel was poured into a PTFE-lined autoclave and put for hydrothermal treatment for 24h and 48h at 200°C, under the autogenous pressure. The autoclaves were cooled down with cold tap water. The products were recovered by filtration, washed with distilled water and dried overnight under vacuum at 80°C. After drying, the samples were ground till powder. Table 2 shows the amounts of reactants used for the synthesis of the mineral.

The effect of the silica source in the preparation of Ni-phyllsilicate was investigated by using APTS instead of silicic acid (Sample RG-004C in Table 2).

Table 2. Compositions of Ni-phyllsilicates (1:1).

Sample name	NiCl ₂ · 6H ₂ O [g]	NaOH _(aq) [ml]	Silicic acid [ml]	Reaction time [h]	APTS [ml]
RG-004A	1,6050	20,250	100	24h	-
RG-004B	1,6050	20,250	100	48h	-
RG-004C	0,8025	10,125	-	24h	1,185

2.4.2 Synthesis of 2:1 Ni-Phyllsilicates

In a typical procedure 0,535 g of NiCl₂ · 6H₂O solution was dissolved in 100 ml of an aqueous solution of silicic acid. This solution was slowly mixed with 11,25 ml of NaOH (1 mol/L) and stirred magnetically for 10 min at room temperature. Then, 28 ml of the gel was poured into a Teflon-lined autoclave and put for hydrothermal treatment for 24h and 48h at 200°C, under the autogenous pressure. The autoclaves were cooled down with cold tap water. The products were collected by filtration, washed with distilled water, and dried overnight under vacuum at 80°C. After drying, samples were in a ground till powder. Table 3 shows the amounts of reactants used for the synthesis of the mineral.

The effect of the silica source in the preparation of Ni-phyllsilicate was investigated by using APTS instead of silicic acid (Sample RG-005C in Table 3).

Table 3. Compositions of Ni-phyllsilicates (2:1).

Sample name	NiCl ₂ · 6H ₂ O [g]	NaOH _(aq) [ml]	Silicic acid [ml]	Reaction time [h]	APTS [ml]
RG-005A	0,5350	11,250	100	24h	-

RG-005B	0,5350	11,250	100	48h	-
RG-005C	0,2675	5,625	-	24h	0,526

2.4.3 Synthesis of Aminopropyl-Ni-Phyllosilicates and PBI@Ni-Phyllosilicates

The synthesis of aminopropyl-modified 2:1 Ni-Phyllosilicate was performed according to Ferreira et. al. (2008) with few modifications as follow. In a typical procedure, 1,745 g (6 mmol) of nickel nitrate hexahydrate was first dissolved in 50 ml water and the solution was stirred magnetically at room temperature for 5 min. Then, the silica sources (APTS and TEOS) were added according the proportions shown in Table 4. This mixture formed a green suspension. To this mixture, 24 ml of aqueous sodium hydroxide solution (0,5 mol/L) was added dropwise under magnetic stirring. The resultant suspension was aged for 4h at 50 °C in oil bath. Then, the suspension was transferred to a PTFE-lined vessel in stainless autoclave and submitted to hydrothermal treatment for 24h at 200 °C under the autogenous pressure. The products were collected by filtration and washed with distilled water till pH ~7 and then dried overnight under vacuum at 80°C. After drying, samples were ground till powder.

For the synthesis of PBI@Ni-Phyllosilicates, the gel was prepared using APTS and TEOS with the following compositions: i) APTS: TEOS = 1: 4, ii) APTS: TEOS = 1: 1, iii) APTS: TEOS = 2: 1 and iv) APTS: TEOS = 4:1. To the final gel, perylene-3,4,9,10-tetracarboxylic dianhydride (PBA) was added with the molar ratio of 2 APTS: 1 PBA and homogenized for 15 min and placed into the PTFE-lined vessels in stainless autoclave. The HTS were performed at 200 °C for 24h. The final solids were collected by filtration and dried overnight under vacuum at 80 °C.

Table 4. Compositions of the gels for the synthesis Ni-phyllsilicates and PBI@Ni-phyllsilicates.

Sample name	Ni (NO ₃) ₂ · 6H ₂ O [g]	H ₂ O [ml]	NaOH (sub) [ml]	APTS [ml]	TEOS [ml]	PBA [g]	NBA [g]
RG-006A	1,746	50	24	1,880	-	-	-
RG-006B	1,745	50	24	1,255	0,59	-	-
RG-006C	1,744	50	24	0,940	0,89	-	-
RG-006D	1,745	50	24	0,470	1,34	-	-
RG-006E	0,698	20	9,6	-	0,714	-	-
RG-006F	0,873	25	12	0,235	0,670	0,2080	-

RG-006G	0,873	25	12	0,235	0,670	-	0,1423
RG-006H	0,872	25	12	0,094	0,803	0,0538	-
RG-006I	0,874	25	12	0,047	0,847	0,0269	-
RG-006J	0,872	25	12	0,470	0,445	0,2693	-
RG-006K	0,873	25	12	0,047	0,847	-	-
RG-006L	0,873	25	12	0,094	0,803	-	-
RG-006M	0,873	25	12	0,094	0,803	-	-
RG-006N	0,873	25	12	0,094	0,803	0,0538	-
RG-006O	0,874	25	12	0,047	0,847	-	-
RG-006P	0,873	25	12	0,047	0,847	0,0269	-
RG-007A	1,745	50	24	0,470	1,340	0,4160	-

2.5 Hydrothermal synthesis of Zn-Phlogopite and PBI@Zn-Phlogopite

In a typical synthesis, 3,49 g of potassium hydroxide (34,3 mmol), 0,72 g of aluminium nitrate nonahydrate (2,86 mmol), 1,58 g of zinc sulfate heptahydrate (5,53 mmol) and 7,5 mmol of silica source (Ludox HS-30, APTS or TEOS) were magnetically stirred in 25 ml of water for 10 minutes at room temperature. The gel of molar composition 1,92 K₂O: 0,08 Al₂O₃: 0,31 ZnO: 0,42 SiO₂: 84 H₂O was stirred for 10 min and transferred to a PTFE – lined vessels (45 ml) in stainless steel autoclave. The hydrothermal synthesis (HTS) have been carried out under autogenous pressure at 200°C for 24h. Table 5 shows the composition of the different gels for the synthesis of Zn-Phlogopite. The products of the synthesis were collected by filtration, rinsed with distilled water till pH ~7 and then dried overnight under vacuum at 80 °C. After drying, the samples were ground till powder.

For the synthesis of PBI@Zn-Phlogopite, the gel was prepared using APTS and/or TEOS with the following compositions: *i*) APTS: TEOS = 1: 4, *ii*) APTS: TEOS = 1: 1, *iii*) APTS: TEOS = 2: 1 and *iv*) APTS: TEOS = 4:1. To the final gel, perylene-3,4,9,10-tetracarboxylic dianhydride (PBA) was added with the molar ratio of 2 APTS: 1 PBA and homogenized for 15 min and placed into the PTFE-lined vessels in stainless autoclave. The HTS were performed at 200 °C for 24h. The final solids were collected by filtration and dried overnight under vacuum at 80 °C.

Table 5. Compositions of the gels for the synthesis of Zn-Phlogopite and PBI@Zn-Phlogopite.

Sample name	KOH [g]	H ₂ O [ml]	ZnSO ₄ · 7H ₂ O [g]	Al (NO ₃) ₃ · 9H ₂ O [g]	Ludox HS 30 [ml]	TEOS [ml]	APTS [ml]	PBA [g]	NBA [g]
RG-002A	3,82	25	1,59	0,72	1,24	-	-	-	-
RG-002B	3,82	25	1,58	0,72	-	1,67	-	-	-
RG-002C	3,84	25	1,58	0,72	-	-	1,75	-	-
RG-002D	3,84	25	1,58	0,72	-	0,836	0,878	-	-
RG-002E	3,84	25	1,58	0,72	0,605	-	0,878	-	-
RG-002F	3,84	25	1,58	0,72	-	-	1,75	1,47	-
RG-002G	3,86	25	1,58	0,72	-	-	1,75	-	1,01
RG-002H	3,82	25	1,58	0,72	-	1,256	0,438	-	-
RG-002I	3,82	25	1,58	0,72	-	1,506	0,1754	-	-
RG-002J	3,82	25	1,58	0,72	-	1,586	0,0845	-	-
RG-002K	3,82	25	1,58	0,72	-	1,586	0,0845	-	-
RG-002L	3,82	25	1,58	0,72	-	1,586	0,0845	0,07	-
RG-002M	3,82	25	1,58	0,72	-	1,586	0,0845	-	0,05
RG-002N	3,85	25	1,58	0,72	-	1,506	0,175	0,1	-
RG-002O	3,81	25	1,58	0,72	-	1,256	0,438	0,25	-
RG-002P	3,85	25	1,58	0,72	-	0,837	0,878	0,5	-

2.6 Characterization

Powder X-ray diffraction (PXRD) data was collected with a PANalytical X'Pert Pro multipurpose diffractometer (MPD) in Bragg Brentano geometry operating with a Cu anode at 40 kV, 40 mA. An X-Celerator multichannel detector was used. The diffraction patterns were recorded between 5 ° and 90 ° (2theta) with 69.215 s/step and a step size of 0.0050134 °.

Attenuated Total Reflectance Fourier Transform InfraRed (ATR-FTIR) spectra were recorded on a PerkinElmer UATR Two with a diamond crystal. Resolution was set to 4 cm^{-1} and spectra were recorded from 4000 to 450 cm^{-1} .

Scanning electron microscopy (SEM) was carried out with a Quanta 200F FEI microscope. Typically, the samples were measured at 5 kV with a working distance of *ca.* 9 mm and spot size 2.5 . Prior to imaging, samples were coated by sputtering a 17 nm thick layer of Au/Pd 60/40 alloy with a Quorum Q105T S sample preparation system.

UV-Vis absorption spectra were recorded in solid state with a Perkin Elmer Lambda 750 spectrometer. Fluorescence emission and excitation were measured in an Edinburgh FLS920 instrument with iris aperture of 100% , dwell of 0.5 s and step of 2 nm . Excitation spectra were obtained at the maxima of the Emission spectra.

All graphs were made using Origin 2018 program.

3. RESULTS AND DISCUSSION

3.1 Gyrolite

Synthetic gyrolites were made using Ludox HS-30 as silica source at 200°C from 24h to 72h. The hydrothermal synthesis of gyrolite was performed successfully as indicated by PXRD (Fig. 9 A). All the samples showed characteristics peaks at *c.a.* 8°, 21°, 25°, 24°, 29°, 32° and 49° 2θ as described by Siauciunas *et al.* (2004). This result indicates that 24h is enough to obtain gyrolite with good crystallinity (Siauciunas & Baltakys, 2004).

For future incorporation of PBA into the mineral, an aminopropyl-group was inserted into the structure of gyrolite. It would play the role of a linker between the inorganic mineral and the organic dye. For this purpose, 3-aminopropyltriethoxysilane (APTS) was used as silica source, together with tetraethylorthosilicate (TEOS) in the following molar ratios: 100% TEOS, 50% TEOS: 50% APTS and 50% APTS: 50% Ludox HS-30. The PXRD patterns of the obtained materials are shown in Fig. 9 B. The PXRD diffractions do not correspond to the structure of gyrolite as observed in Fig. 9 A. Regardless the silica source (APTS: TEOS or APTS: Ludox), the solids present a broad amorphous halos between 20-30 ° 2θ together with peaks assigned to Ca(OH)₂. Since the synthesis of aminopropyl-modified gyrolite did not work, this mineral was not further investigated.

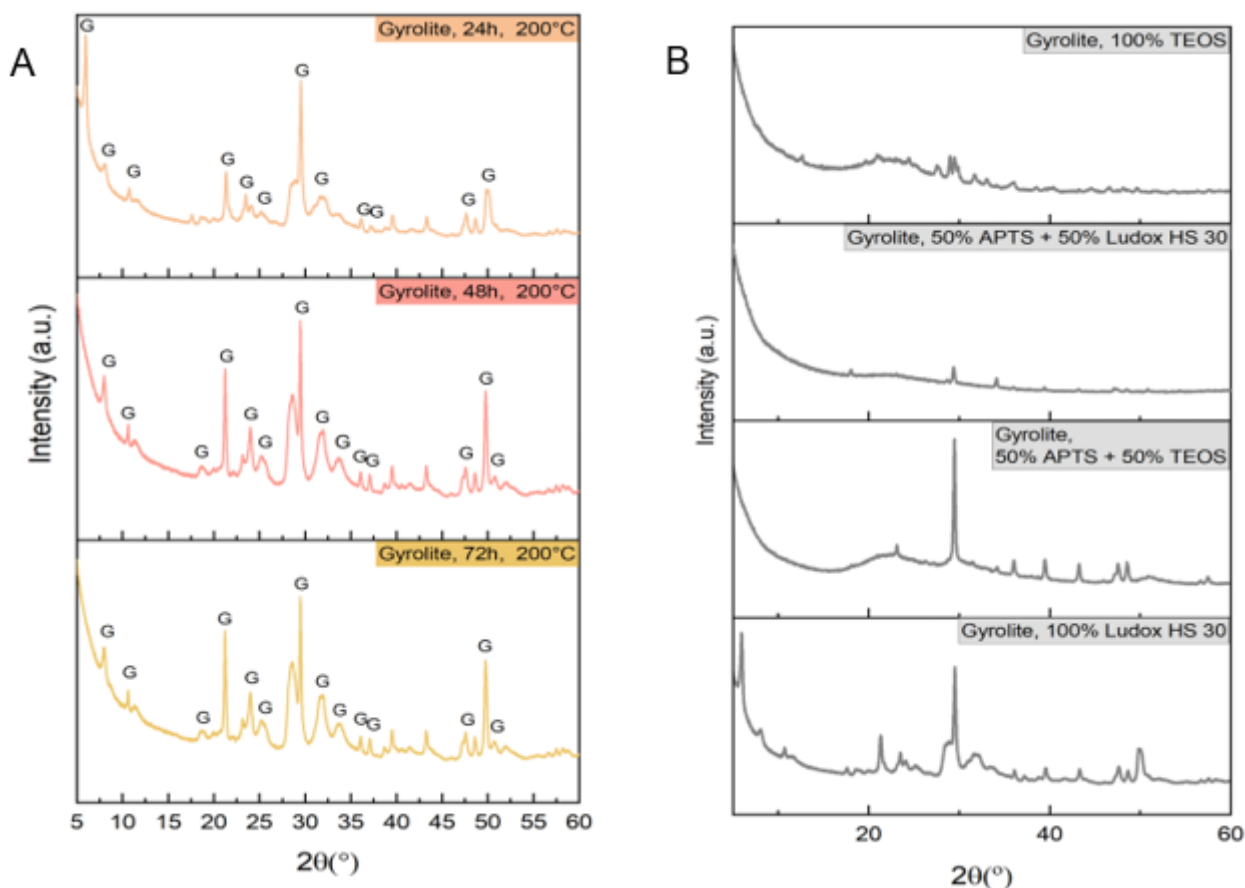


Figure 9. PXRD patterns of synthetic gyrolite: A) using Ludox HS-30, HTS at 200 °C for 24h, 48h, 72h. B) using TEOS/APTS/Ludox HS-30 as silica sources, at 200 °C for 24h. G letters indicate the characteristic peaks of gyrolite.

3.2 Ni-Hectorite

The mineral Ni-Hectorite was synthesized as described by Nakakuki (NAKAKUKI et al., 2005). Fig. 10. shows the PXRD diffractogram of the obtained material. The diffraction peaks do not correspond to the one reported by Nakakuki *et al.*. After a couple of attempts, it was decided not to continue the experiments with this mineral.

Since Ni-Hectorite could not be obtained, Ni-Phyllosilicates were investigated and the synthesis of 1: 1 and 2:1 Ni-Phyllosilicates were performed as described by Mizutani *et al.* (1990). The PXRD diffractograms of Ni-Phyllosilicate 1:1 and 2:1 using water glass or sodium orthosilicate are shown in Fig. 11A and 11B, respectively. It can be observed the typical diffractions described by the authors at around 12°, 28° and 40° 2θ for the mineral 1:1 and 8°, 28° and 40° 2θ for the 2:1.

When the silica source was changed to APTS, the PXRD patterns of the mineral 1:1 (Fig. 11C) and 2:1 (Fig. 11D) show peaks that did not correspond to the original mineral. Having these results in mind, we discontinued the synthesis of Ni-Phyllosilicates 1:1 and 2:1 using the procedure described by Mizutani *et al.* (1990). (Mizutani et al., 1990)

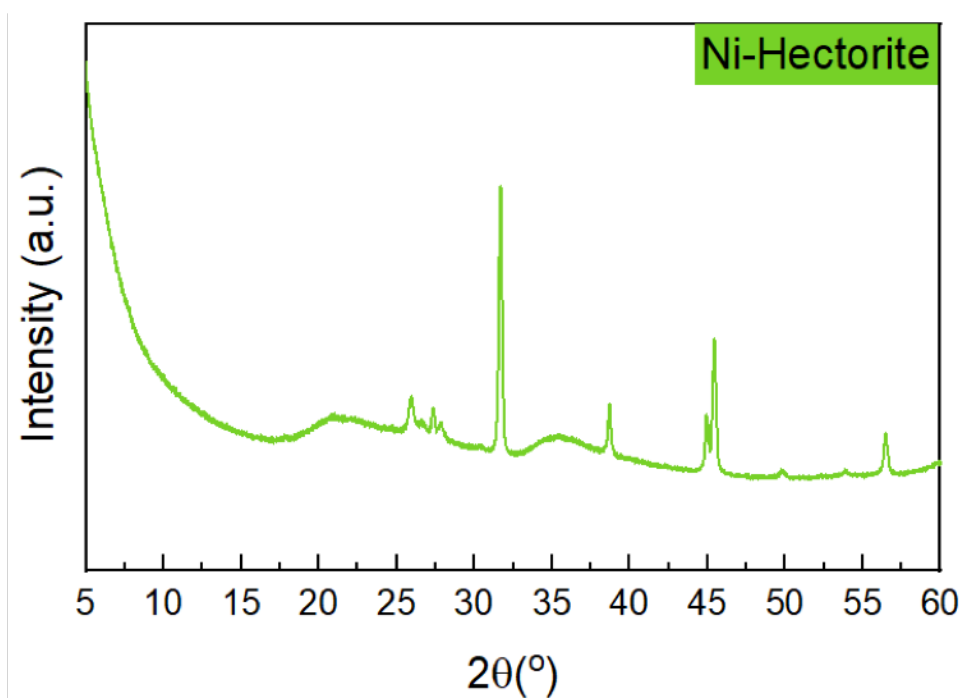


Figure 10. PXRD pattern of Ni-Hectorite.

3.3 Ni-Phyllosilicates

Since Ni-Hectorite could not be obtained, Ni-Phyllosilicates were investigated and the synthesis of 1: 1 and 2:1 Ni-Phyllosilicates were performed as described by Mizutani *et al.* (1990). The PXRD diffractograms of Ni-Phyllosilicate 1:1 and 2:1 using water glass or sodium orthosilicate are shown in Fig. 11A and 11B, respectively. It can be observed the typical diffractions described by the authors at around 12°, 28° and 40° 2q for the mineral 1:1 and 8°, 28° and 40° 2q for the 2:1.

When the silica source was changed to APTS, the PXRD patterns of the mineral 1:1 (Fig. 11C) and 2:1 (Fig. 11D) show peaks that did not correspond to the original mineral. Having these results

in mind, we discontinued the synthesis of Ni-Phyllosilicates 1:1 and 2:1 using the procedure described by Mizutani *et al.* (1990). (Mizutani *et al.*, 1990)

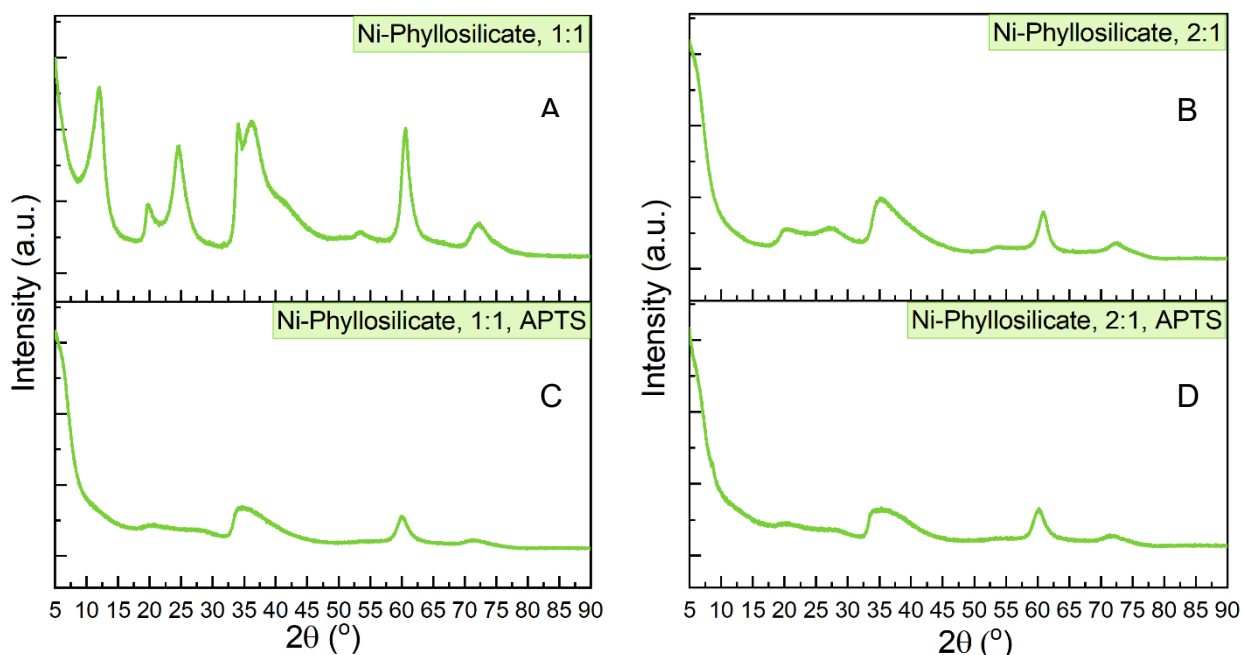


Figure 11. PXRD patterns of Ni-Phyllosilicates by Mizutani *et al.* (1990). A) Ni-Phyllosilicate 1:1, B) Ni-Phyllosilicate 2:1, C) Aminopropyl-modified Ni-Phyllosilicate 1:1 and D) Aminopropyl-modified Ni-Phyllosilicate 2:1.

3.4 Aminopropyl-modified 2:1 Ni-Phyllosilicates and PBI@Ni-Phyllosilicates

Aminopropyl-modified 2:1 Ni-Phyllosilicates were obtained by hydrothermal synthesis as described by Ferreira *et al.* (2008), but instead of using magnesium nitrate hexahydrate was used nickel nitrate as metal source. Different molar ratios APTS: TEOS were investigated: *i*) 5% APTS: 95% TEOS, *ii*) 10% APTS: 90% TEOS, *iii*) 25% APTS: 75% TEOS and *iv*) 50% APTS: 50% TEOS. A second set of reactions was prepared by adding perylene bisanhydride (PBA) to the gel of aminopropyl-modified 2:1 Ni-Phyllosilicates previously to the HTS, in order to form perylene bisimide (PBI) dyes within the mineral, *i.e.*, the hybrid material PBI@Ni-Phyllosilicates.

Figure 12 A-D show the pictures of the crude aminopropyl-modified 2:1 Ni-Phyllosilicates while Fig. 12 E-H present the colors of PBI@Ni-Phyllosilicates. The color of aminopropyl-modified Ni-Phyllosilicates changes from light green to dark red once the organic dye is present. Visually, the darkness of the PBI@Ni-Phyllosilicates hybrid materials increases as the amount of $-NH_2$ groups available to react with PBA decreases (5% APTS).

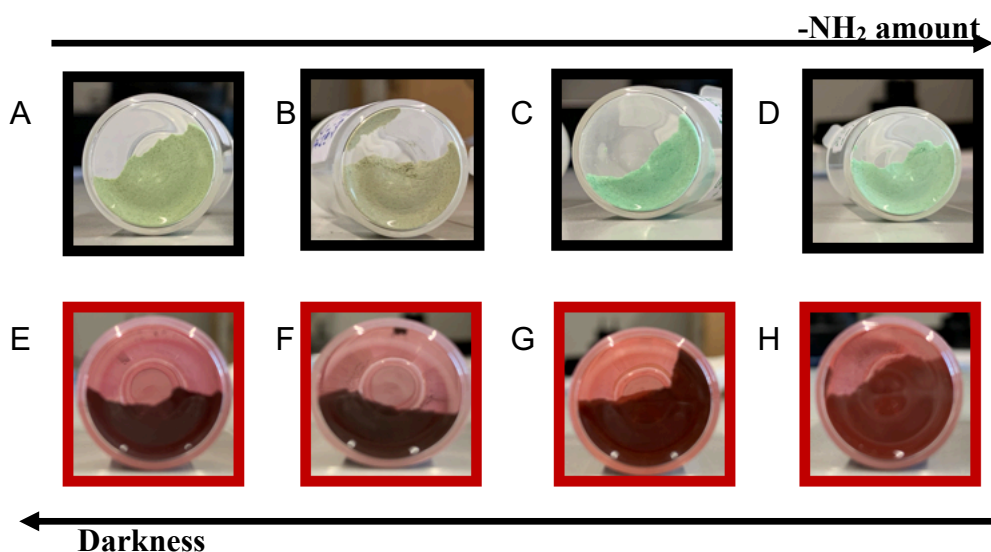


Figure 12. Colors of the crude aminopropyl Ni-Phyllosilicates without dye: A) 5% APTS, B) 10% APTS, C) 25% APTS and D) 50% APTS. Colors of the crude PBI@Ni-Phyllosilicates: E) 5% APTS + PBA, F) 10% APTS + PBA, G) 25% APTS + PBA and H) 50% APTS + PBA.

3.4.1 The crystallinity of aminopropyl-modified Ni-Phyllosilicates and their hybrid materials by PXRD

Aminopropyl-modified Ni-phyllsilicates and the hybrid materials PBI@Ni-phyllsilicates were analysed by PXRD and their diffractograms are seen in Fig. 13. At lower amounts of aminopropyl groups present in the mineral (APTS: TEOS of 5 and 10%, Fig. 13A and 13B, respectively) the solids present sharp diffractions peaks at $19,28^\circ$, $33,12^\circ$, $38,60^\circ$ and $52,17^\circ$ 2θ , indicated by asterisks. These are assigned to the presence of nickel hydroxide (Tong et al., 2012), precipitated during the synthesis of the mineral which was not washed enough for these samples. When PBA is added to the synthesis in order to form PBI@Ni-Phyllosilicate, the peaks from $\text{Ni}(\text{OH})_2$ have their intensity decreased.

The minerals containing 25 and 50% of APTS (Fig. 13 C and 13 D, respectively) show the typical diffractogram of this class of minerals at around 24° , 35° and 60° 2θ , assigned to the plans (020), (003) and (060), respectively, typical of talc structures (Dumas et al., 2013). The (060) reflection was observed at 0.154 nm for all the minerals prepared with APTS; this value is characteristic of a trioctahedral 2: 1 phyllosilicate structure (in the octahedral sheets each O atom or OH group is surrounded by three divalent cations (Jaber et al., 2005).

By adding PBA to the synthesis of the minerals containing 25 and 50% of APTS, red curves in Fig. 13 C and D, the peaks of the hybrid materials are maintained at same positions, indicating that the addition of PBA does not influences the formation of the mineral. On the other hand, it can be observed aggregates of non-reacted PBA in the solid made with the highest amount of aminopropyl

groups, red curve in Fig. 13 D. Regarding the interlayer space of these solids, it should be necessary to analyze them at lower angles.

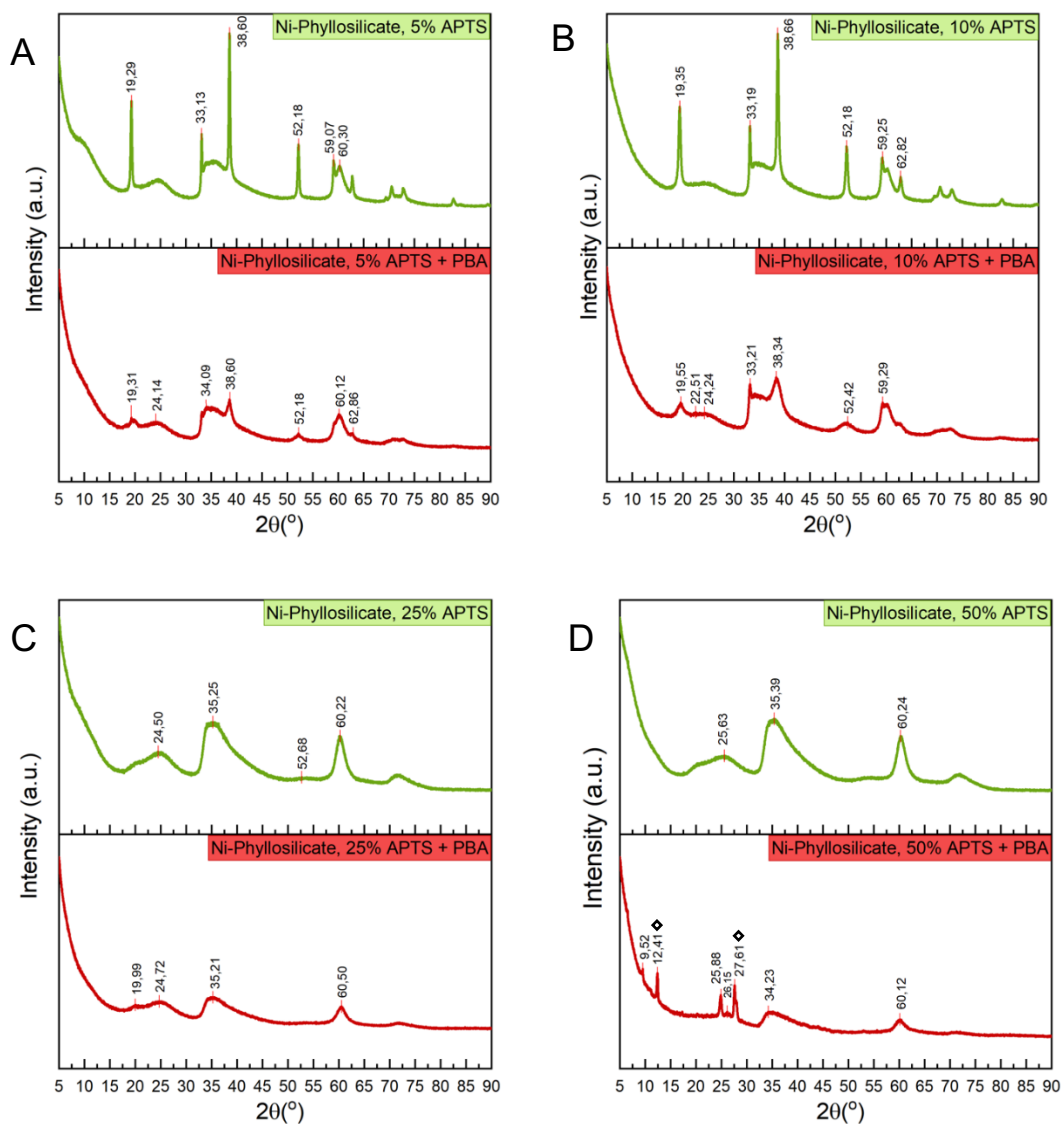


Figure 13. PXRD patterns of aminopropyl-modified Ni-Phyllosilicates and PBI@Ni-Phyllosilicates. Minerals containing aminopropyl groups with A) 5% APTS, B) 10% APTS, C) 25% APTS and D) 50% APTS are seen in green lines. Their respective hybrid materials PBI@Ni-Phyllosilicates are shown in red. *Ni(OH)₂ ♦PBA aggregates

3.4.2 The local order of aminopropyl-modified Ni-Phyllosilicates and their hybrid materials by ATR-FTIR

The structure of the aminopropyl-modified Ni-Phyllosilicate was also illustrated by ATR-FTIR spectra. The green curves in Fig. 14 A-D show the infrared spectrum of the minerals containing APTS with 5, 10, 25 and 50%, respectively.

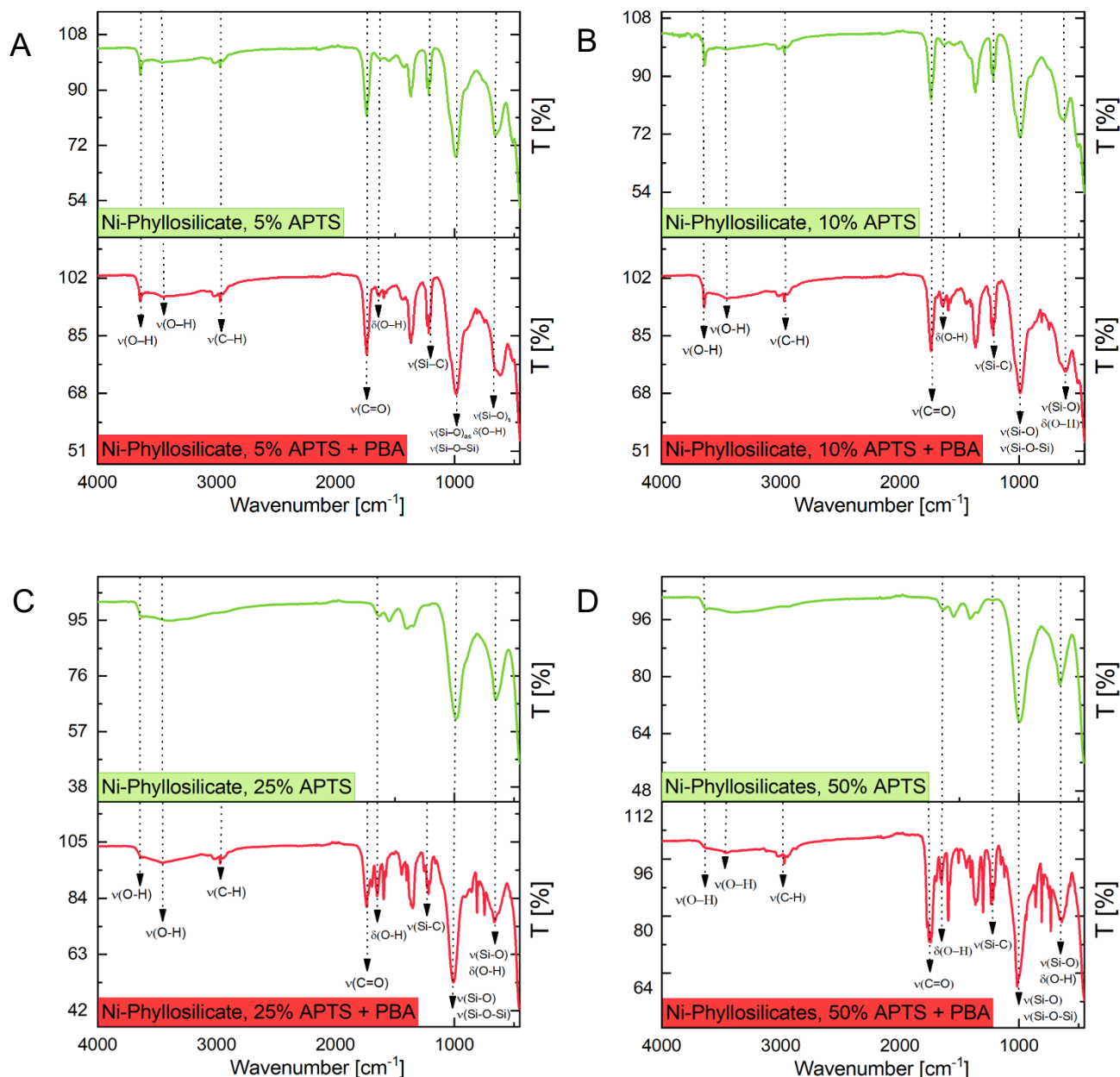


Figure 14. ATR-FTIR spectra of the aminopropyl-modified Ni-Phyllosilicates and PBI@Ni-Phyllosilicates. Minerals containing aminopropyl groups with A) 5% APTS, B) 10% APTS, C) 25% APTS and D) 50% APTS are seen in green lines. Their respective hybrid materials PBI@Ni-Phyllosilicates are shown in red.

All the aminopropyl-modified minerals exhibit two bands due to the presence of the physisorbed water, namely the ν (O-H) stretching frequency at 3440 cm^{-1} and the δ (O-H) deformation band at 1640 cm^{-1} . It presented also characteristic vibration bands of talc structure at 3640 cm^{-1} for ν (O-H) in Ni-OH group, at 1030 cm^{-1} for the overlap of ν (Si-O)_{as} and ν (Si-O-Si), at 673 cm^{-1} for the overlap of ν (Si-O)_s and δ (O-H) (Martin et al., 1999). The organic content is indicated by the appearance of a ν (Si-C) vibration as a shoulder in the range $1197\text{--}1212\text{ cm}^{-1}$. In the minerals containing 25 and 50% of APTS, it can be observed a decrease of intensity of the ν (O-H)

band assigned to ν (O–H) in Ni–OH group, which implies that more APTS reacted the Ni–OH groups as expected. For all aminopropyl-modified Ni-Phyllosilicates, CH stretching vibrations of the propyl chain appeared at 2947–2952 and 2897–2904 cm^{-1} for asymmetric and symmetric ν (C–H), respectively.

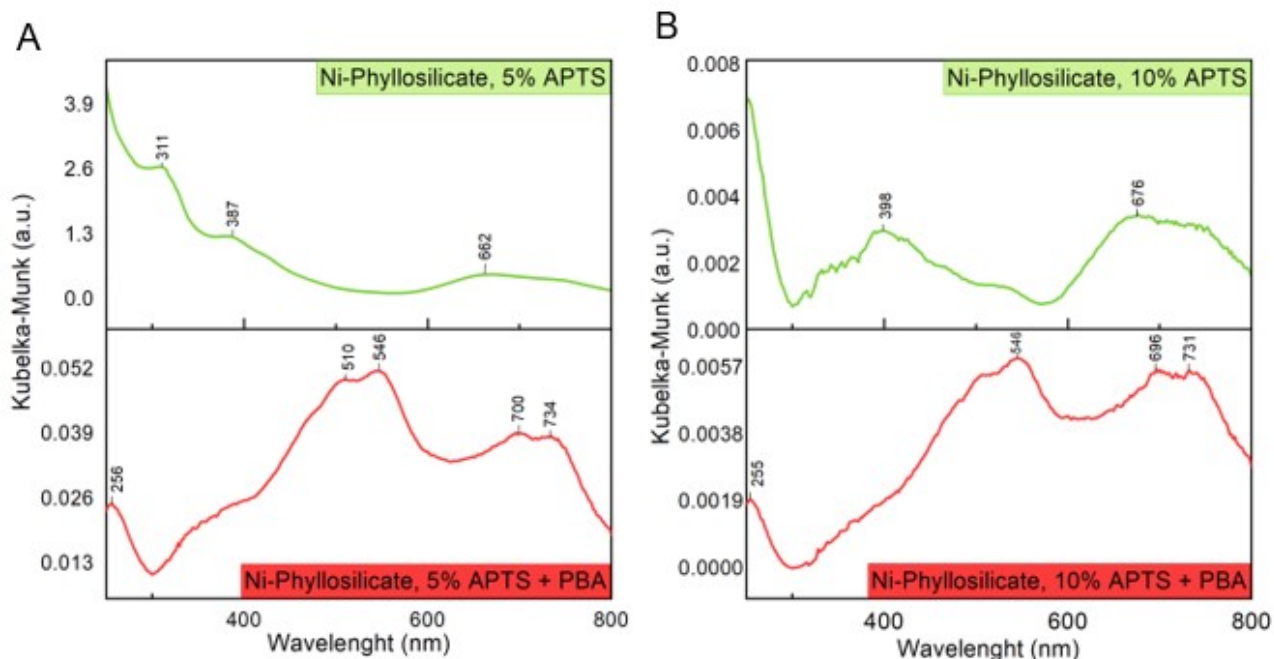
The hybrid materials PBI@Ni-Phyllosilicates were also analyzed by ATR-FTIR and their spectra are seen in the red curves of Fig. 14 A-D. In all cases, it can be observed that the most intense band is ν (Si–O–Si) at around 1000 cm^{-1} and the appearance of a broad band at 1740 cm^{-1} assigned to the ν (C=O) from PBA. However, the presence of imide modes from the desired perylene bisimide (PBI) can't be observed at *c.a.* 1690 and 1650 cm^{-1} . Indeed, the strong δ (O–H) band of the water can overlap the ν (C–N) vibration. In this case, ^{13}C NMR spectroscopy could be an important tool to elucidate the structure.

3.4.3 UV measurements

The UV-Vis spectra of the aminopropyl-Modified Ni-Phyllosilicates with and without PBA are shown in Fig.15.

All the minerals containing APTS, green curves in Fig 15 A-D, present absorbances at around 387 nm and 662 nm which are assigned to nickel (Sun et al., 2006).

When PBA is added to the synthesis of the minerals, red curves in Fig. 15 A-D, it can be observed absorbances at *c.a.* 255 nm, 510 nm, 545 nm, 700 nm and 735 nm, which are assigned to PBA. (D'Souza & Kadish, 2011)



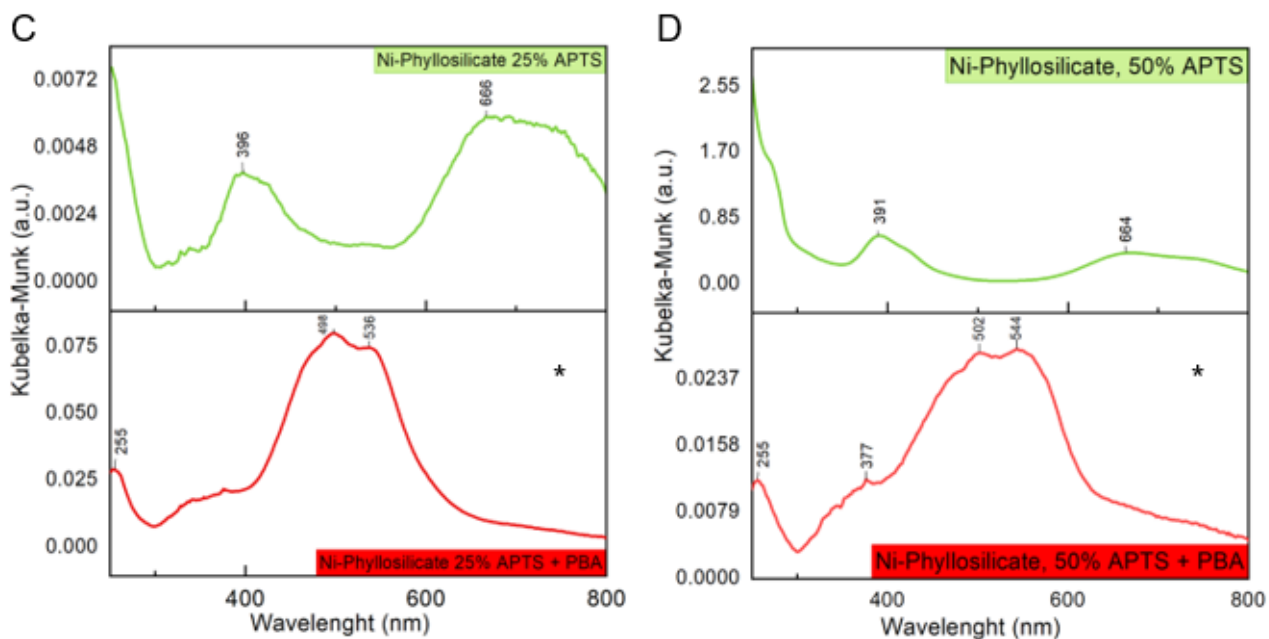


Figure 15. UV-Vis spectra of the aminopropyl-modified Ni-Phyllosilicates and PBI@Ni-Phyllosilicates. Minerals containing aminopropyl groups with A) 5% APTS, B) 10% APTS, C) 25% APTS and D) 50% APTS are seen in green lines. Their respective hybrid materials PBI@Ni-Phyllosilicates are shown in red. *in BaSO₄

3.4.4 Fluorescence

The fluorescence properties of the aminopropyl-modified Ni-Phyllosilicates with and without PBA are shown in Fig. 16. Fig. 16 A shows the spectra of aminopropyl-modified Ni-Phyllosilicate synthesized with 5% of APTS. The peaks observed are not in agreement with the color observed for the green powder. It might be an artefact and should be remeasured. When PBA is added to the synthesis of the mineral, the fluorescence spectra of the hybrid material, Fig. 16 B, it presents an emission peak at 706 nm (red region) and excitation at 642 nm (orange-red region).

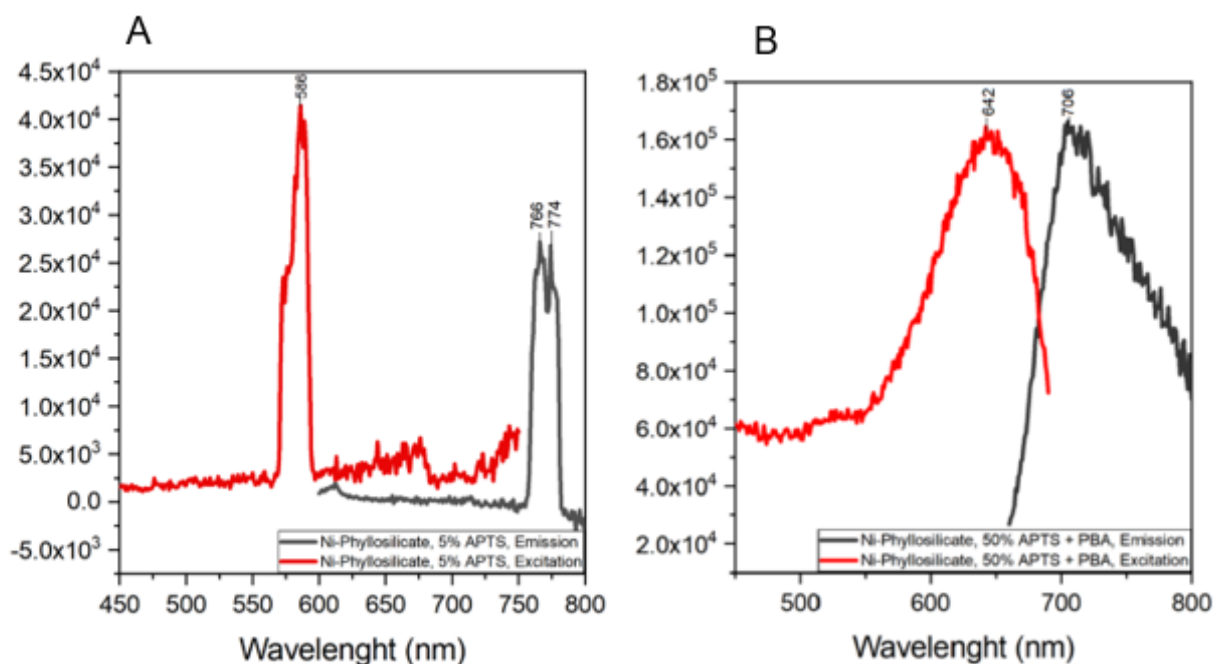


Figure 16. The fluorescence measurements of synthesized Aminopropyl – modified Ni – Phyllosilicates with and without PBA dye: A) 5% APTS without PBA and B) 50% APTS with PBA.

3.4.5 Morphology of aminopropyl-modified Ni-Phyllosilicates and their hybrid materials

Figure 17 shows the morphology of the Ni-Phyllosilicates and their hybrid materials obtained by SEM.

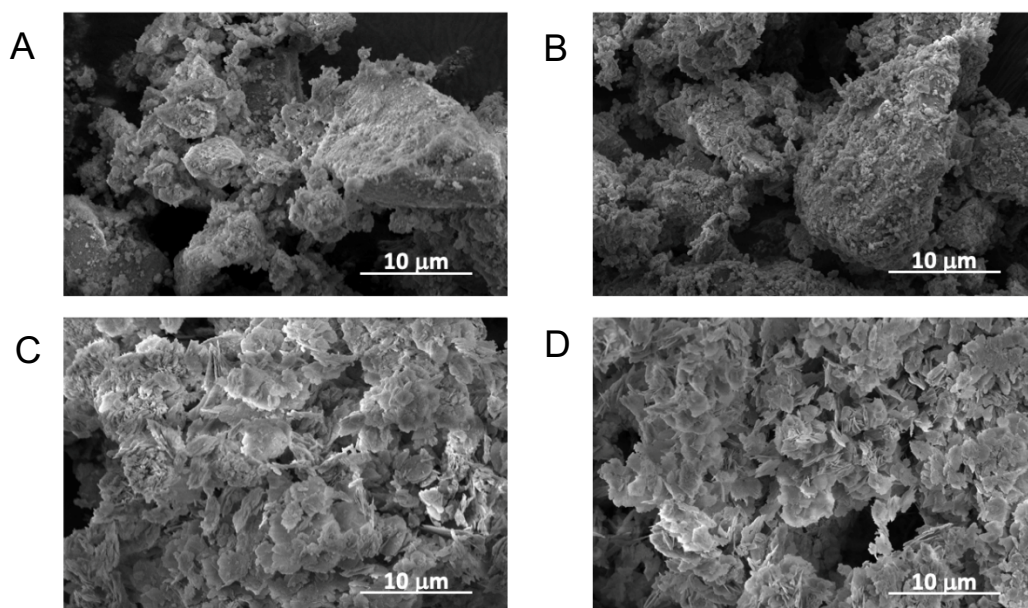


Figure 17. Scanning electron microscopy (SEM) of aminopropyl-modified Ni-Phyllosilicates and their hybrid materials. A) 100% APTS, without dye; B) 50% APTS, with PBA dye; C) 5% APTS, without dye; D) 5% APTS, with PBA dye.

In figures 17 A and 17 B is clearly seen a difference between different concentrations of APTS. In photos where concentration of APTS is 50% or 100% sample looks like solid aggregates. In figure 17 B, where the material is with PBA dye, no difference was seen comparing with Ni-Phyllosilicate which had no dye added, but still high percentage of APTS (17 A).

Ni-Phyllosilicates with small amounts of APTS (5%), Fig. 17 C, have cornflake morphology, which is typically observed for natural clay minerals, especially for phyllosilicates (Reinholdt et al., 2013). In the presence of PBA, Fig. 17 D, the morphology of the mineral is maintained.

3.5 Zn-Phlogopite and PBI@Zn-Phlogopite

Zn – Phlogopites were obtained by hydrothermal synthesis as described by (Mcguire et al., 2014) and (Perrotta & Garland, 1975). Figure 18 shows that samples A, B, C, D, E without dyes, are all white. Color of dyed samples 18 F, G, H, I, J was getting lighter when the concentration of APTS and PBA dye was smaller: 5% APTS with PBA dye was the whitest and 50% APTS with PBA dye was most rosy.

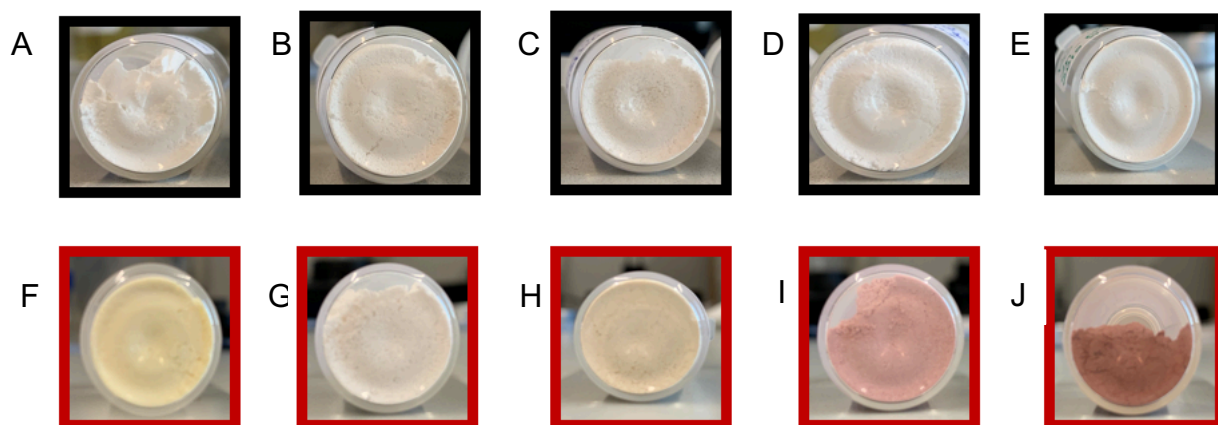


Figure 18. Colors of synthesized Zn – Phlogopite. A) 5% APTS; B) 10% APTS; C) 25% APTS; D) 50% APTS; E) 100% APTS; F) 5% APTS + PBA; G) 10% APTS + PBA; H) 25% APTS + PBA; I) 50% APTS + PBA; J) 100% APTS + PBA;

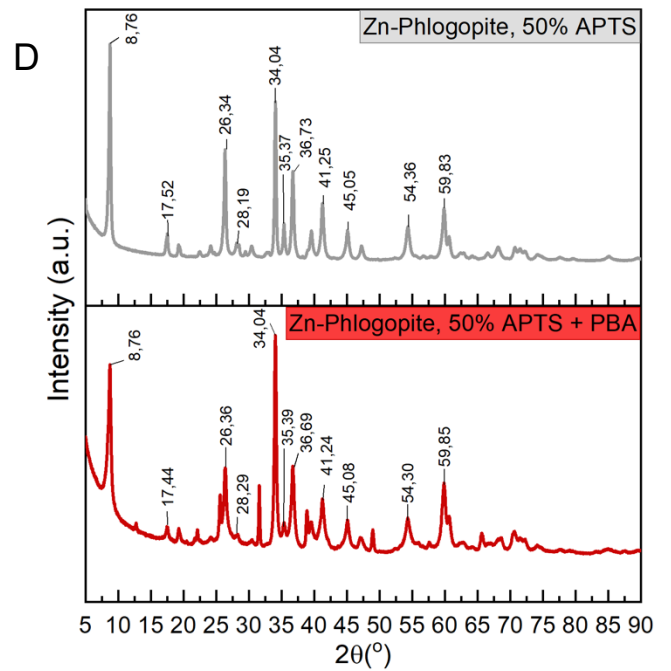
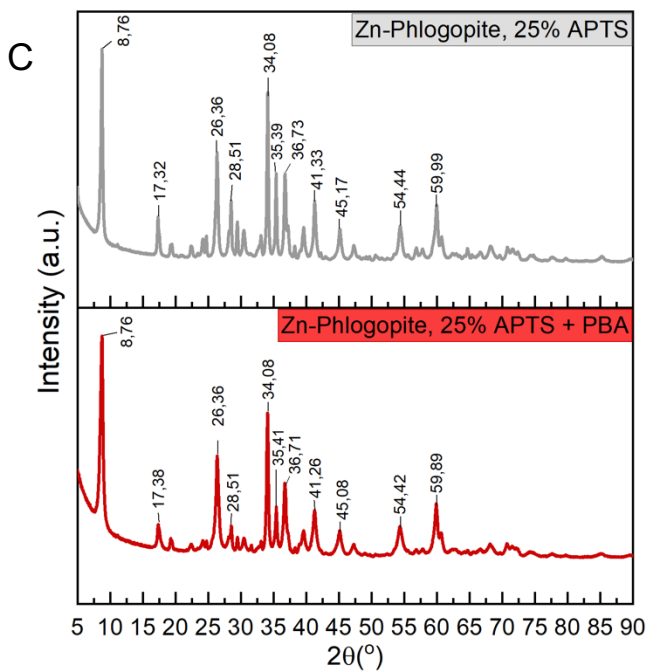
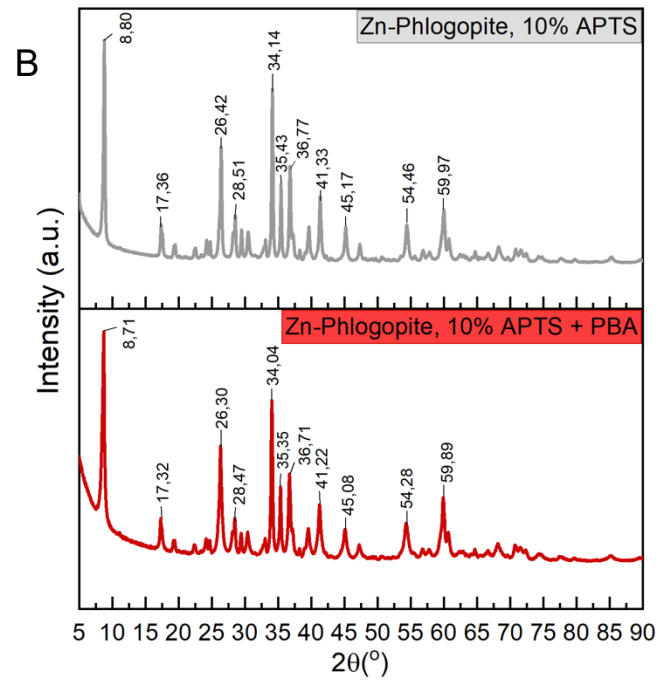
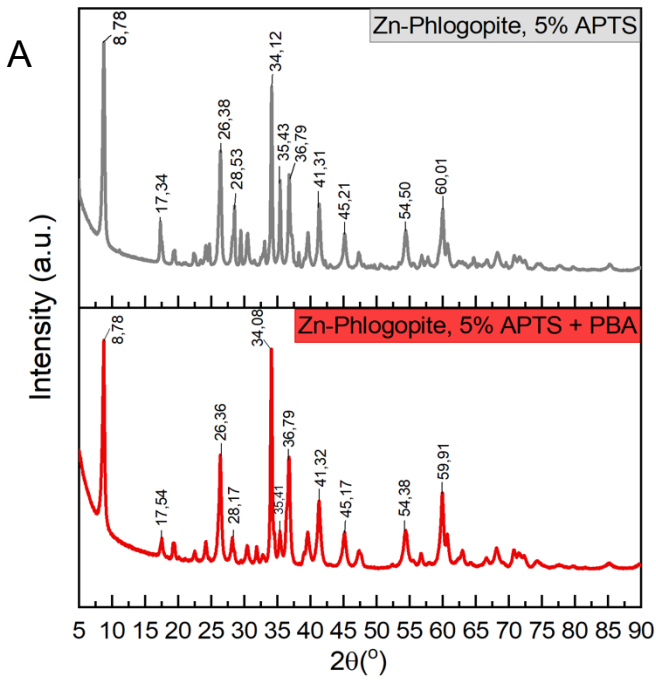
3.5.1 The crystallinity of Zn-Phlogopite and their hybrid materials by PXRD

Zinc phlogopite and the hybrid materials PBI@Zn-Phlogopite were analyzed by PXRD and their diffractograms are seen in figure 19.

Figure 19 A without dye most intense peaks are at $8,78^{\circ} 2\theta$, $26,38^{\circ} 2\theta$, $34,12^{\circ} 2\theta$ and $36,79^{\circ} 2\theta$. The first peak d value is $11,18 \text{ \AA}$. In figure 19 B material sample without PBA dye shows most intense peaks at $8,80^{\circ} 2\theta$, $26,42^{\circ} 2\theta$, $34,14^{\circ} 2\theta$, $36,77^{\circ} 2\theta$ and its first peak d value is $11,15 \text{ \AA}$. In figures 19 C and 19 D, samples without dyes show the same first peaks and the same d value, which are $8,76^{\circ} 2\theta$, $d=11,20 \text{ \AA}$. Figure 13 C shows highest peaks at $8,76^{\circ} 2\theta$, $26,36^{\circ} 2\theta$, $34,08^{\circ} 2\theta$, $36,73^{\circ} 2\theta$ and d value is $11,20 \text{ \AA}$. In figure 19 D where sample was made with 50% APTS, without dye highest peaks are at $8,76^{\circ} 2\theta$, $26,34^{\circ} 2\theta$, $34,04^{\circ} 2\theta$ and $36,73^{\circ} 2\theta$, d value of first peak is $d=11,20 \text{ \AA}$. Figure 19 E, sample with 100% APTS, d value of the first peak is $11,20 \text{ \AA}$ and most intense peaks are at $8,76^{\circ} 2\theta$, $26,34^{\circ} 2\theta$, $34,07^{\circ} 2\theta$, $36,71^{\circ} 2\theta$. After comparing these results to Zi-Phlogopite patent, corresponded peaks were at the same positions (Mcguire et al., 2014).

In figure 19 A, where the sample was made with 5% APTS and PBA dye, most intense peaks are at $8,78^{\circ} 2\theta$, $26,36^{\circ} 2\theta$, $34,08^{\circ} 2\theta$, $36,79^{\circ} 2\theta$, d of the first peak is $11,18 \text{ \AA}$. After synthesis with PBA dye, some of the intense peaks compared with the sample without dye decreased, peaks are at $17,54^{\circ} 2\theta$, $28,17^{\circ} 2\theta$ and $35,41^{\circ} 2\theta$. Figure 19 B with PBA dye shows peaks at $8,71^{\circ} 2\theta$, $26,30^{\circ} 2\theta$, $34,04^{\circ} 2\theta$, $36,71^{\circ} 2\theta$, $d=11,26 \text{ \AA}$. Decreased peaks after adding organic dye $17,32^{\circ} 2\theta$, $28,47^{\circ} 2\theta$ and $35,35^{\circ} 2\theta$. In figure 19 C, where the sample was made with 25% APTS and PBA dye, most intense peaks are at $8,76^{\circ} 2\theta$, $26,36^{\circ} 2\theta$, $34,08^{\circ} 2\theta$, $36,71^{\circ} 2\theta$, d value of the first peak is $11,20 \text{ \AA}$ and decreased peaks are at $17,38^{\circ} 2\theta$, $28,51^{\circ} 2\theta$, $34,39^{\circ} 2\theta$ and $41,33^{\circ} 2\theta$. Figure 19 D with PBA dye shows highest peaks at $8,76^{\circ} 2\theta$, $26,36^{\circ} 2\theta$, $34,04^{\circ} 2\theta$ and $36,69^{\circ} 2\theta$, and its first peak d value is $11,20 \text{ \AA}$. The peaks which decreased after adding PBA are at $17,44^{\circ} 2\theta$, $26,36^{\circ} 2\theta$, $28,29^{\circ} 2\theta$ and $35,39^{\circ} 2\theta$. In figure 19 E, where was a sample with 100% of APTS and PBA, most intense peaks are at $8,70^{\circ} 2\theta$, $26,32^{\circ} 2\theta$, $34,04^{\circ} 2\theta$ and $36,67^{\circ} 2\theta$ and its first peak d value is $11,27 \text{ \AA}$. After synthesis

with PBA dye, some of the intense peaks decreased, peaks are at $17,46^\circ 2\theta$, $28,15^\circ 2\theta$, $35,33^\circ 2\theta$ and $45,03^\circ 2\theta$. Most of the peaks after adding the perylene dye did not change positions drastically.



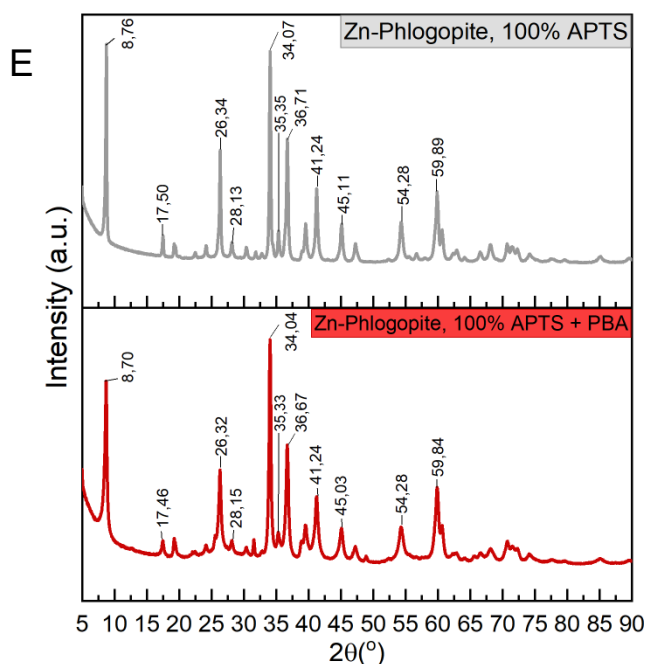


Figure 19. The XRD diffraction patterns of Zn - Phlogopite. Comparison between with (red)/without(grey) PBA dye: A) 5% APTS; B) 10% APTS; C) 25% APTS; D) 50% APTS; E) 100%.

3.5.2 The local order of Zinc phlogopite and their hybrid materials by ATR-FTIR

The infrared spectra with Fourier transformation of the synthesized Zn – Phlogopites are shown in Figure 20.

In all figures 20 A, B, C, D, samples without organic PBA dye had only one very intense band which presents also characteristic vibration bands of talc structure at 950 cm^{-1} for the overlap of $\nu(\text{Si-O})_{\text{as}}$ and $\nu(\text{Si-O-Si})$. At 3670 cm^{-1} was a very weak $\nu(\text{OH})$.

All hybrid materials PBI@Zn-Phlogopite in figure 20 A, B, C, D (red graphs) shows the same three bands. The first one is most intense $\nu(\text{Si-O-Si})$ at around 950 cm^{-1} , the second one is a broad band at 1730 cm^{-1} assigned to the $\nu(\text{C=O})$ from PBA and the third one shows weak $\nu(\text{OH})$ at 3670 cm^{-1} .

The C=O band was found only in all Zn – Phlogopite samples with PBA dye. We can see anhydride bond $\nu(\text{C=O})$, but there is no imide mode from perylene bisimide (PBI) at 1690 and 1650 cm^{-1} to be indicated.

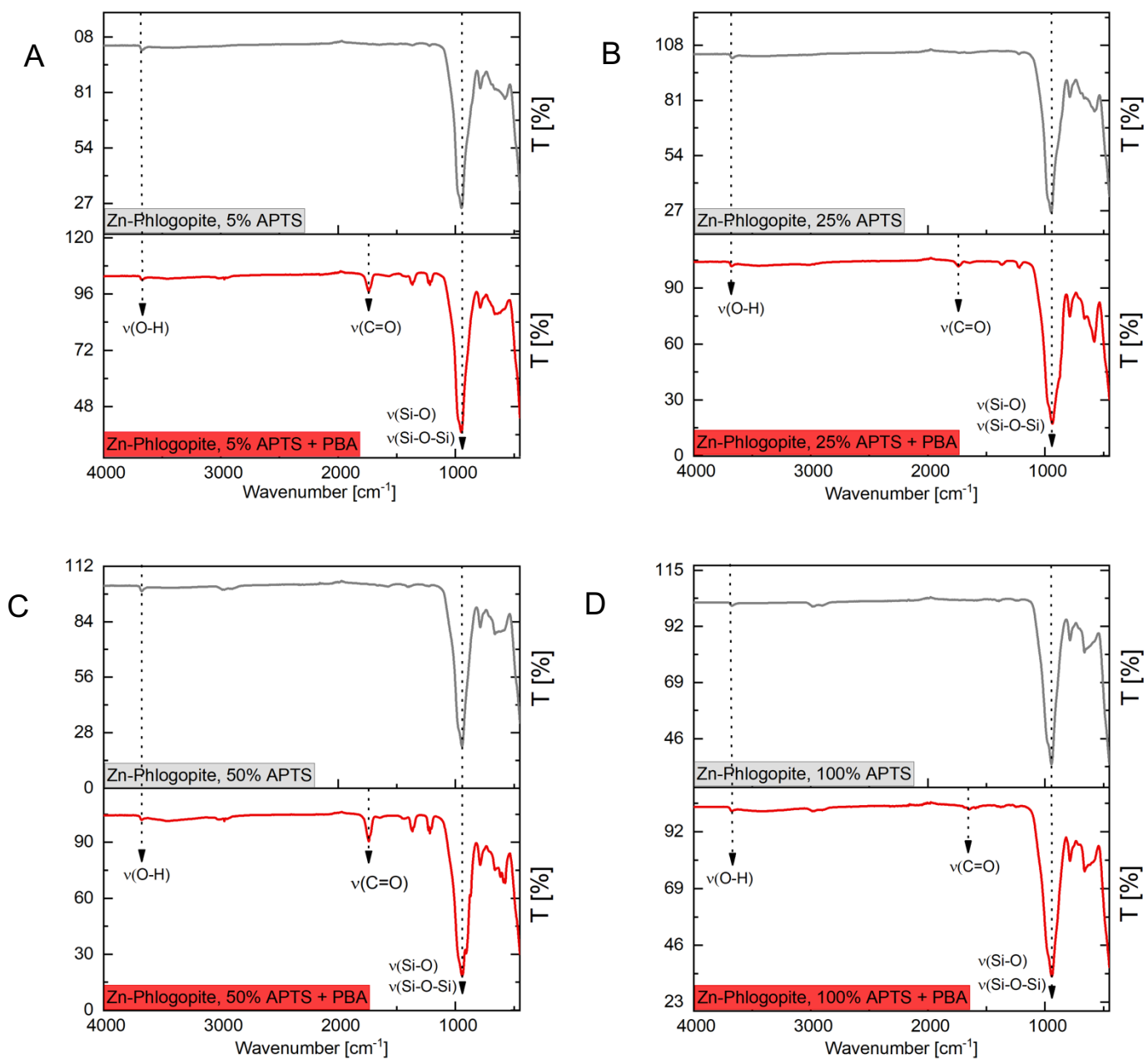


Figure 20. Infrared spectra from the synthesized Zn – Phlogopites. Comparison between with (red)/without (grey) PBA dye: a) 5% APTS; b) 25% APTS; c) 50% APTS; d) 100% APTS.

3.5.3 UV measurements

The UV-Vis measurements of synthesized Zn – Phlogopite with and without PBA dye, are shown in Figure 21.

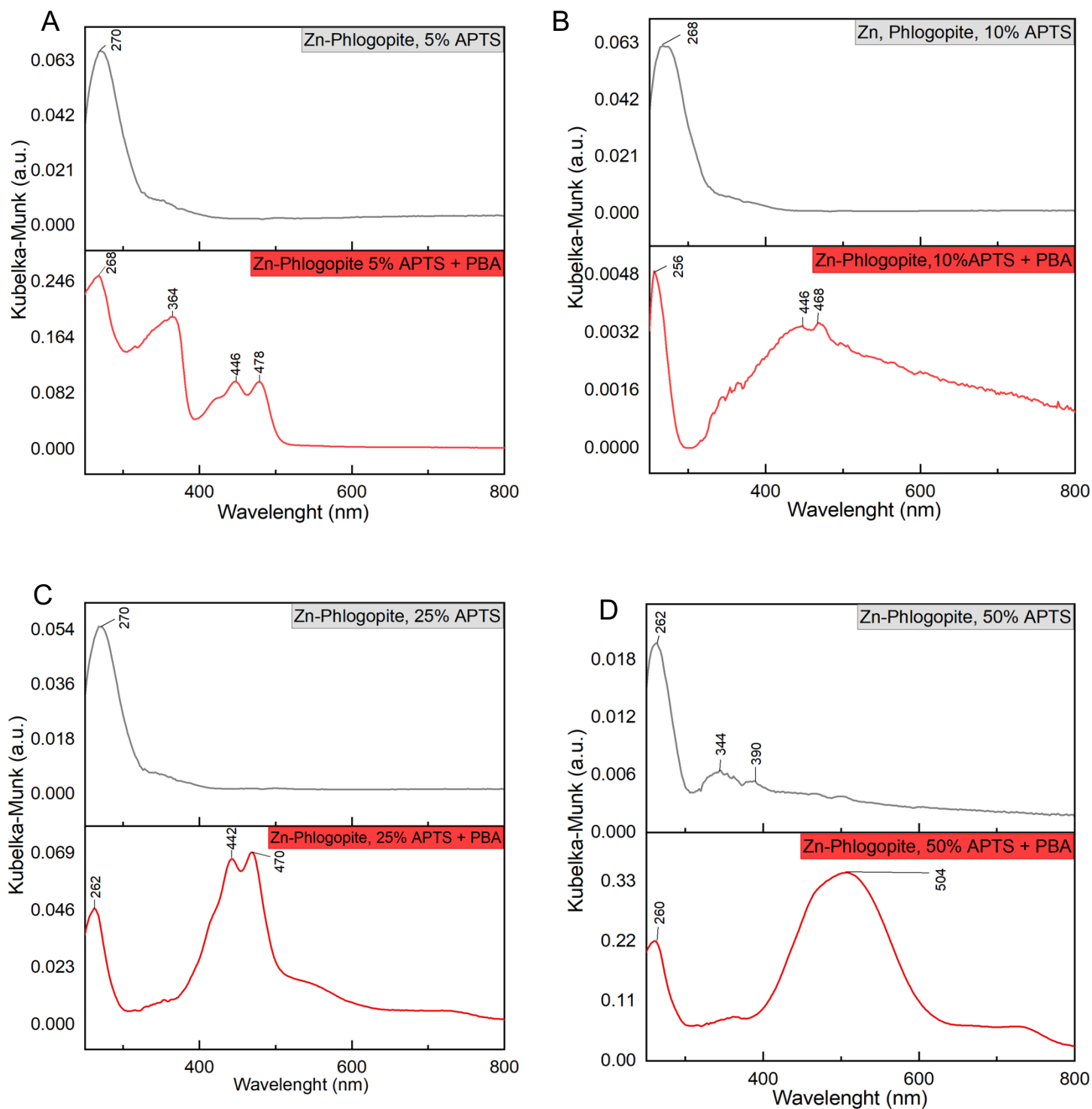


Figure 21. UV-Vis measurements of Zn - Phlogopite. Comparison between with (red) /without (grey) PBA dye: a) 5% APTS; b) 10% APTS; c) 25% APTS; d) 50% APTS.

In all graphs we do see one peak which is around 250-270 nm and it indicates that all synthesized Zn – Phlogopites are naturally fluorescent at UV wavelength. In figure 21 A and 21 C at 270 nm (UV region), in figure 21 B 268 nm, 20 D figure without dye has more than one peak compared to other Zn – Phlogopites without dye, the main peak is at 262 nm and other peaks are at 344nm and 384 nm (UV region).

In pattern 21 A of 5% APTS with PBA dye Zn – Phlogopite we see three more peaks which are at 268 nm (UV), 364 nm (UV), 446 nm (blue) and 478 nm (cyan). Figure 21 B shows that in PBI@Zn-Phlogopite, which has 10% of APTS, has more peaks, which look more edgy and it has a higher background, but the main two peaks from dye are at 446 nm and 468 nm (blue-cyan), and from phlogopite at 256 nm (UV). In Figure 21 C, hybrid, which contains of 25% of APTS and PBA dye, main peaks are at 268 nm, 442 nm and 470 nm (blue-cyan). In Figure 21 D, sample, which was made with 50% APTS and PBA dye, peaks are at 260 nm (UV) and 504 nm (blue – green). In all of these hybrid materials with the dye peaks from 440 nm to 510 nm comes from PBI (Pan et al., 2015)(Baumgartner et al., 2017).

Intensive broad peaks at 260 – 270 nm can be related to charge transfer from zinc-phlogopite to PBA ligand.

3.5.4 Fluorescence

The fluorescent measurements of synthesized Zn – Phlogopite with and without PBA dye, are shown in Figure 22.

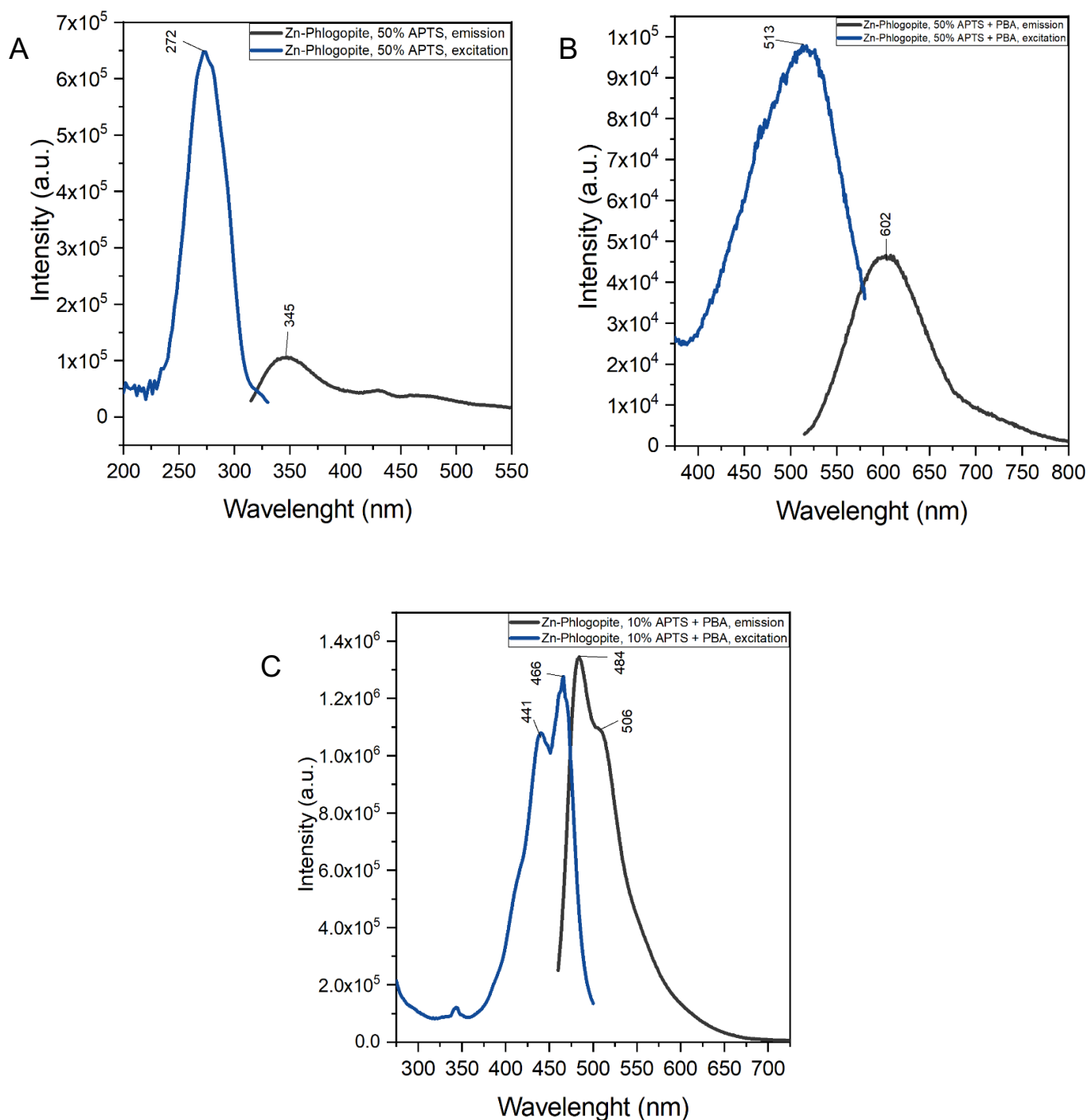


Figure 22. The fluorescent measurements of synthesized Zn – Phlogopite with and without PBA dye: A) 50% APTS B) 50% APTS with PBA C) 10% APTS with PBA.

Figure 22 A shows Zn – Phlogopite was synthesized without PBA dye. It shows that emission at this sample is at 345 nm and excitation is at 272 nm. In figure 22 B Zn – Phlogopite was synthesized with 50% APTS and PBA dye and the sample showed emission at 602 nm (orange) and excitation at 513 nm (green). Figure 22 C shows Zn – Phlogopite synthesized with 10% APTS and PBA dye. It shows that emission at this sample is at 484 nm (cyan) and 506 nm (green), excitation is at 441 nm and 466 nm (UV region).

3.5.5 Morphology of Zn-Phlogopites and their hybrid materials

Figure 23 shows the morphology of the Zn – Phlogopites and their hybrid materials. In figures 23 A and 23 C photos show that if it does not contain PBA dye the morphology structure is like natural clay - looking like cornflakes or sand – rose. (Reinholdt et al., 2013). In photos 23 B and 23 D After adding PBA dye structure changes a little bit and looks like crust or crashed cornflakes, pieces become smaller.

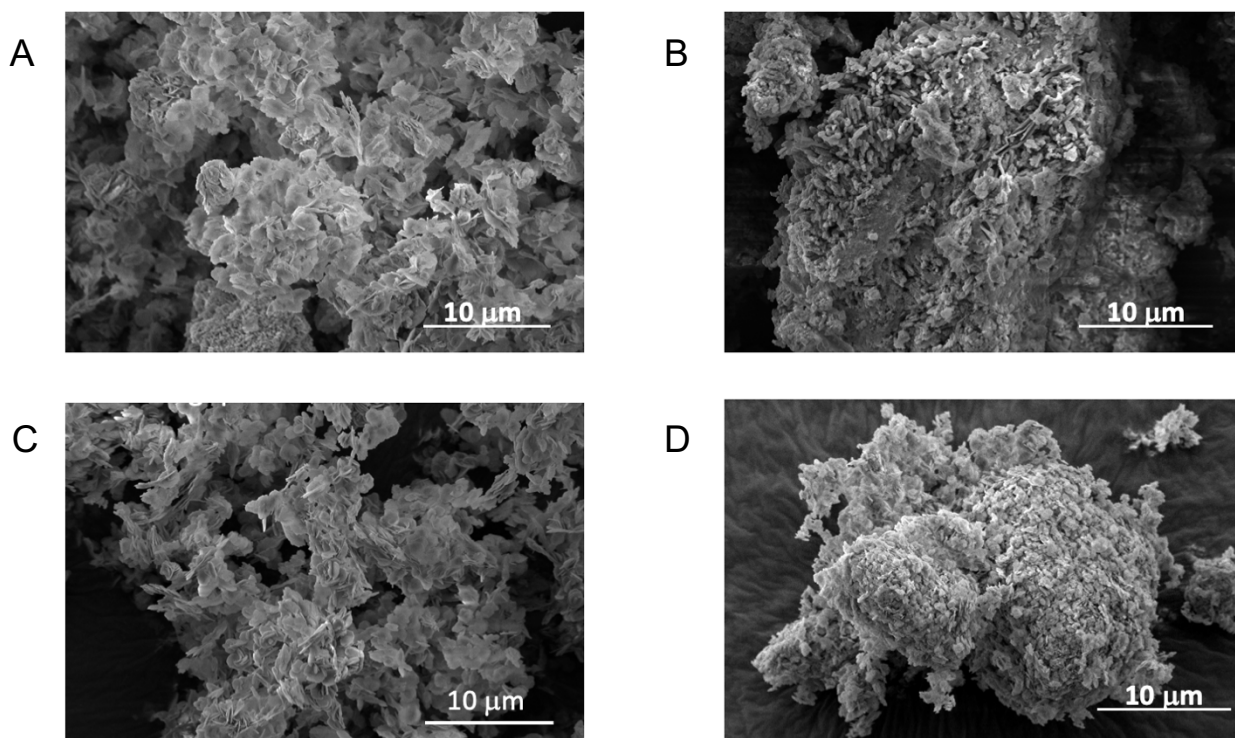


Figure 23. Scanning electron microscopy (SEM) of Zn – Phlogopites and their hybrid materials. A) 5% APTS, without dye; B) 5% APTS, with PBA dye; C) 50% APTS, without dye; D) 50% APTS, with PBA dye.

4. CONCLUSION AND OUTLOOK

1. The synthesis of four different fluorescent minerals concomitantly with the synthesis of perylene bisimide dyes (PBI) by one pot hydrothermal synthesis, seems to be promising for only two minerals: Ni-phyllsilicate and Zn-phlogopite.

2. In order to bind the organic dye into the mineral surface, their standard synthesis was modified by using aminopropyltriethoxysilane (APTS) and tetraethylorthosilicate (TEOS) as silica source. Simple modifications of Ni-phyllsilicates with aminopropyl groups showed to be a good approach to future incorporate anhydride dyes as PBA. Aminopropyl-modified Ni-Phyllsilicates and Zn-Phlogopite keep their PXRD patterns and contains the aminopropyl groups as indicated by FTIR.

3. Aminopropyl-modified Ni-Phyllsilicates and Zn-Phlogopites were prepared using APTS as silica source in different APTS: TEOS ratios and perylene-3,4,9,10-tetracarboxylic dianhydride (PBA) were added to their synthesis. PXRD of both types of hybrid materials (PBI@Ni-Phyllsilicates and PBI@Zn-Phlogopites) are similar to their corresponding aminopropyl-modified mineral without dye.

4. It was observed that the presence of PBA does not disturb the crystallization of the inorganic phase. However, ATR-FTIR has showed to be inadequate to confirm the presence of imide modes assigned to the organic PBI, only intense absorbances from PBA modes are seen. In both types of mineral, the morphologies of the hybrid materials are kept as cornflakes, typical of natural clays.

5. The UV-Vis spectra of PBI@Ni-Phyllsilicates hybrid materials showed peaks at 255 nm and 540 nm. Fluorescence results show that the excitation and emission peaks are at the red region. The UV-Vis spectra of aminopropyl-modified Zn-Phlogopites showed peaks at 265 nm which change to 450 nm and 500 nm when PBA is added to their synthesis. Fluorescence measurements showed that the aminopropyl-modified mineral interact with light at around 270 nm, *i.e.*, they are intrinsically fluorescent. By adding PBA to their synthesis, it could be observed that the emission and excitation shifted to the red region, indicating the change in the fluorescent behaviour of the mineral.

6. Further researches of these hybrid materials could focus on the synthesis parameters and deep characterization of the imide's units of the dye component. Moreover, the understanding of intercalation capacity, surface reactivity, and biocompatibility would lead to future applications such as in pharmacy and drug delivery systems.

5. REFERENCES

- Al-Khateeb, B., Dinleyici, M., Abourajab, A., K k, C., Bodapati, J. B., Uzun, D., Koyuncu, S., & Icil, H. (2020). Swallow tail bay-substituted novel perylene bisimides: Synthesis, characterization, photophysical and electrochemical properties and DFT studies. *Journal of Photochemistry and Photobiology A: Chemistry*, 393, 112432. <https://doi.org/10.1016/j.jphotochem.2020.112432>
- Ash, I., & Ash, M. (2007). *Handbook of Fillers, Extenders, and Diluents*. 503. https://books.google.lt/books?id=C4Cr8dHupVsC&pg=PA298&lpg=PA298&dq=phlogopite+pharmaceuticals&source=bl&ots=3V5O1Mzzqo&sig=ACfU3U25DjdK_1UmKcd2cV6rnRwJfGHHgw&hl=lt&sa=X&ved=2ahUKEwihY-Bo9DpAhXowqYKHc_iClgQ6AEwD3oECAQQAQ#v=onepage&q=phlogopite+pharmaceut
- Baumgartner, B., Svirikova, A., Binting, J., Hametner, C., Marchetti-Deschmann, M., & Unterlass, M. M. (2017). Green and highly efficient synthesis of perylene and naphthalene bisimides in nothing but water. *Chemical Communications*, 53(7), 1229–1232. <https://doi.org/10.1039/c6cc06567h>
- Bleam, W. (2017). Clay Mineralogy and Chemistry. In *Soil and Environmental Chemistry*. <https://doi.org/10.1016/b978-0-12-804178-9.00003-3>
- Borovik, S. A. (1989). FLUORESCENT METHODS. In *GEOCHEMICAL AND MINERALOGICAL METHODS OF PROSPECTING FOR MINERAL DEPOSITS CHAPTER IV, SPECIAL METHODS OF PROSPECTING* (Vol. 4, pp. 24–26). https://books.googleusercontent.com/books/content?req=AKW5QaeZb8cCzW14I5L5LPBCISJJgAXxJxcIOIe9Nj7iGbkyHgkrSKm9_f_eQZBmoPJ-LQQeri7eZdQbiBrACMUvmaq8k5jh-CyOT97vEdjCbC9lZkltWgy565ZnSag8m-cDJYIEGvgQupUrfpQ872PWSk2UuDKmw2c-wbLtqk2HWF2IP_ywlLi4L6KmLa7khGsKsla
- Bostwick, R. (1992). The Check-list of Franklin-Sterling Hill Fluorescent Minerals: Discussion and Update. *The Picking Table Journal of the Franklin-Ogdensburg Mineralocigal Society, INC.*, 33(2), 4–12. www.FOMSNJ.org
- Brady, K. (2010). *Luminescence , fluorescence and phosphorescence of minerals*. 2010. <https://www.fluomin.org/uk/fiche.php?id=388>
- Brigatti, M. F., Gal n, E., & Theng, B. K. G. (2013). Structure and Mineralogy of Clay Minerals. In *Developments in Clay Science* (Vol. 5). <https://doi.org/10.1016/B978-0-08-098258-8.00002-X>
- Chheda, T. D., Mookherjee, M., Mainprice, D., Dos Santos, A. M., Molaison, J. J., Chantel, J., Manthilake, G., & Bassett, W. A. (2014). Structure and elasticity of phlogopite under compression: Geophysical implications. *Physics of the Earth and Planetary Interiors*, 233, 1–12. <https://doi.org/10.1016/j.pepi.2014.05.004>
- Cilek, V. (2009). *Earth System: History and Natural Variability - Volume I*. EOLSS Publishers Company Limited. <https://books.google.lt/books?id=kJ9nCwAAQBAJ>
- D’Souza, F., & Kadish, K. M. (2011). *Handbook of Carbon Nano Materials* (Vol. 2). WORLD SCIENTIFIC. <https://doi.org/10.1142/7976>
- DeMent, J. (2014). *Handbook of Fluorescent Gems and Minerals: An Exposition and Catalog of the Fluorescent and Phosphorescent Gems and Minerals, Including the Use of Ultraviolet Light in the Earth Sciences*. <https://books.google.lt/books?id=VuN9CgAAQBAJ&pg=PT71&lpg=PT71&dq=gyrolite+fluorescence&source=bl&ots=j8cA5HpCGV&sig=ACfU3U1qD3in0KsK4vs7SpxYmgrHKUcRhg&hl=lt&sa=X&ved=2ahUKEwjG2-3-jsvpAhXi->

yoKHaZZA90Q6AEwA3oECAkQAQ#v=onepage&q=gyrolite fluorescence&f=fals

- Dumas, A., Martin, F., Le Roux, C., Micoud, P., Petit, S., Ferrage, E., Brendlé, J., Grauby, O., & Greenhill-Hooper, M. (2013). Phyllosilicates synthesis: A way of accessing edges contributions in NMR and FTIR spectroscopies. Example of synthetic talc. *Physics and Chemistry of Minerals*, 40(4), 361–373. <https://doi.org/10.1007/s00269-013-0577-5>
- Feng, B., Zhang, W., Guo, Y., Peng, J., Ning, X., & Wang, H. (2018). Synergistic effect of acidified water glass and locust bean gum in the flotation of a refractory copper sulfide ore. *Journal of Cleaner Production*, 202, 1077–1084. <https://doi.org/10.1016/j.jclepro.2018.08.214>
- Ferreira, R. B., Silva, R., & Pastore, H. O. (2008). *Aminopropyl-Modified Magnesium-Phyllosilicates Layered Solids.pdf*. 7, 14215–14221.
- Fish, J. C., & Agoston, G. A. (1980). Color Theory and Its Application in Art and Design. *Leonardo*, 13(4), 333. <https://doi.org/10.2307/1578122>
- Flint, E. P., McMurdie, H. F., & Wells, L. S. (1938). Formation of hydrated calcium silicates at elevated temperatures and pressures. *Journal of Research of the National Bureau of Standards*, 21(5), 617. <https://doi.org/10.6028/jres.021.034>
- Gaft, M., Reneta, R., & Panczer, G. (2015). *Modern Luminescence Spectroscopy of Minerals and Materials - Michael Gaft, Renata Reisfeld, Gerard Panczer - Google Books*. https://books.google.it/books?id=btkLCwAAQBAJ&pg=PA579&lpg=PA579&dq=Artificial+mineral+identical+to+their+natural+counterparts.&source=bl&ots=6Yuc6giiys&sig=ACfU3U1CzWXog23SfQq-HjCN18vfvYHN6g&hl=lt&sa=X&ved=2ahUKEwiNt5qk8MrpAhW_wcQBHcCMAA8Q6AEwB3oECAcQAQ#
- Gârea, S. A., Voicu, A. I., & Iovu, H. (2017). Clay-Polymer Nanocomposites for Controlled Drug Release. In *Clay-Polymer Nanocomposites*. <https://doi.org/10.1016/B978-0-323-46153-5.00014-8>
- Gyrolite - Collection Arkane*. (n.d.). Retrieved May 24, 2020, from <https://collectionarkane.com/fluorescent-minerals/135-prehnite.html>
- Hawthorne, F. C., Uvarova, Y. A., & Sokolova, E. (2019). A structure hierarchy for silicate minerals: sheet silicates. *Mineralogical Magazine*, 83(1), 3–55. <https://doi.org/10.1180/mgm.2018.152>
- Jaber, M., Miéché-Brendlé, J., Delmotte, L., & Le Dred, R. (2005). Formation of organoclays by a one step synthesis. *Solid State Sciences*, 7(5), 610–615. <https://doi.org/10.1016/j.solidstatesciences.2005.02.003>
- Langhals, H. (1985). Synthese von hochreinen Perylen-Fluoreszenzfarbstoffen in großen Mengen – gezielte Darstellung von Atrop-Isomeren. *Chemische Berichte*, 118(11), 4641–4645. <https://doi.org/10.1002/cber.19851181138>
- Lavikainen, L. (2016). *The structure and surfaces of 2 : 1 phyllosilicate clay minerals The structure and surfaces of* (Vol. 137, Issue 137). http://epublications.uef.fi/pub/urn_isbn_978-952-61-2122-2/urn_isbn_978-952-61-2122-2.pdf
- Martin, F., Micoud, P., Delmotte, L., Marichal, C., Le Dred, R., De Parseval, P., Mari, A., Fortuné, J. P., Salvi, S., Béziat, D., Grauby, O., & Ferret, J. (1999). The structural formula of talc from the Trimouns deposit, Pyrenees, France. *Canadian Mineralogist*, 37(4), 997–1006.
- Mcguire, M. C., Bull, I., Johnson, G. M., & Cordola, E. (2014). *Synthetic zinc phlogopite via Hydrothermal preparation*. <http://www.freepatentsonline.com/y2014/0251202.html>
- Mizutani, T., Fukushima, Y., Okada, A., & Kamigaito, O. (1990). Synthesis of Nickel and

- Magnesium Phyllosilicates with 1:1 and 2:1 Layer Structures. In *Bulletin of the Chemical Society of Japan* (Vol. 63, Issue 7, pp. 2094–2098). <https://doi.org/10.1246/bcsj.63.2094>
- Modreski, P. J., & Aumente-Modreski, R. (1996). Fluorescent Minerals. *Rocks & Minerals*, 71(1), 14–22. <https://doi.org/10.1080/00357529.1996.11761532>
- Mukherjee, S. (2011). Applied Mineralogy. *Applied Mineralogy*, 136–154. <https://doi.org/10.1007/978-94-007-1162-4>
- NAKAKUKI, T., HIRAHARA, H., AISAWA, S., TAKAHASHI, S., & NARITA, E. (2005). HYDROTHERMAL SYNTHESIS AND PHYSIOCHEMICAL PROPERTIES OF Ni-HECTORITE. *Clay Science*, 13(1), 19–26. <https://doi.org/10.11362/jessjclayscience1960.13.19>
- Nelson, S. A. (2015). *Phyllosilicates (Sheet Silicates)*. <https://www.tulane.edu/~sanelson/eens211/phyllosilicates.htm>
- Newsome, D. (1998). Understanding Ultraviolet Lights : A Rockhound's Guide to UV Equipment. *Rock & Gem*, 425, 1–11.
- Pan, L., Ban, J., Lu, S., Chen, G., Yang, J., Luo, Q., Wu, L., & Yu, J. (2015). Improving thermal and mechanical properties of epoxy composites by using functionalized graphene. *RSC Advances*, 5(74), 60596–60607. <https://doi.org/10.1039/c5ra09410k>
- Perrotta, A. J., & Garland, T. J. (1975). Low Temperature Synthesis of Zinc - Phlogopite. *American Mineralogist*, 60, 152–154. [https://doi.org/10.1016/S0167-577X\(97\)00060-8](https://doi.org/10.1016/S0167-577X(97)00060-8)
- Peterson, M., Guide, F., Frederick, H., & Trade, H. (1996). A Field Guide to Rocks and Minerals. In *The Peterson Field Guide Series*. [https://books.google.lt/books?id=C-7APnYVG04C&pg=PA309&dq=Minerals+are+usually+associated+with+rocks&hl=lt&sa=X&ved=0ahUKEwjU0KKRx8rpAhUE7aYKHZfbAYEQ6AEIJzAA#v=onepage&q=Minerals are usually associated with rocks&f=false](https://books.google.lt/books?id=C-7APnYVG04C&pg=PA309&dq=Minerals+are+usually+associated+with+rocks&hl=lt&sa=X&ved=0ahUKEwjU0KKRx8rpAhUE7aYKHZfbAYEQ6AEIJzAA#v=onepage&q=Minerals+are+usually+associated+with+rocks&f=false)
- Rabenau, A. (1985). The Role of Hydrothermal Synthesis in Preparative Chemistry. *Angewandte Chemie International Edition in English*, 24(12), 1026–1040. <https://doi.org/10.1002/anie.198510261>
- Reinholdt, M., Brendlé, J., Tuilier, M.-H., Kaliaguine, S., & Ambroise, E. (2013). Hydrothermal Synthesis and Characterization of Ni-Al Montmorillonite-Like Phyllosilicates. *Nanomaterials*, 3(1), 48–69. <https://doi.org/10.3390/nano3010048>
- Rostami-Tapeh-Esmail, E., Golshan, M., Salami-Kalajahi, M., & Roghani-Mamaqani, H. (2020). Perylene-3,4,9,10-tetracarboxylic diimide and its derivatives: Synthesis, properties and bioapplications. *Dyes and Pigments*, 180, 108488. <https://doi.org/10.1016/j.dyepig.2020.108488>
- Saha, J., Datta Roy, A., Dey, D., Chakraborty, S., Bhattacharjee, D., Paul, P., & Arshad Hussain, S. (2015). Investigation of Fluorescence Resonance Energy Transfer between Fluorescein and Rhodamine 6G. *SPECTROCHIMICA ACTA PART A: MOLECULAR AND BIOMOLECULAR SPECTROSCOPY*, 149, 143–149. <https://doi.org/10.1016/j.saa.2015.04.027>
- Shunmugasamy, V. C., Xiang, C., & Gupta, N. (2015). Clay/Polymer Nanocomposites: Processing, Properties, and Applications. In *Hybrid and Hierarchical Composite Materials*. <https://doi.org/10.1007/978-3-319-12868-9>
- Siauciunas, R., & Baltakys, K. (2004). Formation of gyrolite during hydrothermal synthesis in the mixtures of CaO and amorphous SiO₂ or quartz. *Cement and Concrete Research*, 34(11), 2029–2036. <https://doi.org/10.1016/j.cemconres.2004.03.009>
- Sun, K. Q., Marceau, E., & Che, M. (2006). Evolution of nickel speciation during preparation of Ni-

- SiO₂ catalysts: Effect of the number of chelating ligands in [Ni(en)_x(H₂O)_{6-2x}]²⁺ precursor complexes. *Physical Chemistry Chemical Physics*, 8(14), 1731–1738. <https://doi.org/10.1039/b513319j>
- Taylor S.R. (1964). Abundance of chemical elements in the continental crust: a new table. *Geochimica et Cosmochimica Acta*, 28, 1273–1285.
- Tong, G. X., Liu, F. T., Wu, W. H., Shen, J. P., Hu, X., & Liang, Y. (2012). Polymorphous α- And β-Ni(OH)₂ complex architectures: Morphological and phasal evolution mechanisms and enhanced catalytic activity as non-enzymatic glucose sensors. *CrystEngComm*, 14(18), 5963–5973. <https://doi.org/10.1039/c2ce25622c>
- Türkmen, G., Erten-Ela, S., & Icli, S. (2009). Highly soluble perylene dyes: Synthesis, photophysical and electrochemical characterizations. *Dyes and Pigments*, 83(3), 297–303. <https://doi.org/10.1016/j.dyepig.2009.05.014>
- Valapa, R. B., Loganathan, S., Pugazhenti, G., Thomas, S., & Varghese, T. O. (2017). *An Overview of Polymer / Clay Nanocomposites An Overview of Polymer / Clay Nanocomposites. January.*
- Valeur, B., & Berberan-Santos, M. N. (2011). A brief history of fluorescence and phosphorescence before the emergence of quantum theory. In *Journal of Chemical Education* (Vol. 88, Issue 6, pp. 731–738). <https://doi.org/10.1021/ed100182h>
- Yang, G., & Park, S. J. (2019). Conventional and microwave hydrothermal synthesis and application of functional materials: A review. In *Materials* (Vol. 12, Issue 7, p. 1177). MDPI AG. <https://doi.org/10.3390/ma12071177>
- Zhang, J., Zhou, C. H., Petit, S., & Zhang, H. (2019). Hectorite: Synthesis, modification, assembly and applications. *Applied Clay Science*, 177(October 2018), 114–138. <https://doi.org/10.1016/j.clay.2019.05.001>
- Zussman, J. (1979). The crystal chemistry of the micas. *Bulletin de Minéralogie*, 102(1), 5–13. <https://doi.org/10.3406/bulmi.1979.7243>

SUMMARY

VILNIUS UNIVERSITY
FACULTY OF CHEMISTRY AND GEOSCIENCES

RŪTA GERULAITYTĖ

PERYLENE DYES AT NATURAL FLUORESCENT MINERALS: ROUTE TOWARDS HYBRID MATERIALS VIA ONE POT HYDROTHERMAL SYNTHESIS

Four fluorescent minerals from the Phyllosilicates family were prepared and modified with organic chromophores in order to change their fluorescent behaviours. The incorporation of organic perylene-3,4,9,10-tetracarboxylic dianhydride (PBA) during the crystallization of the minerals by one-pot hydrothermal synthesis was attempted. All the minerals and their corresponding hybrids were analysed by SEM, PXRD, ATR-FTIR, UV-Vis and Fluorescence spectroscopies. Gyrolite and Ni-Hectorites do not allow the incorporation of organic groups on their structures. As indicated by XRD, their crystalline structures can not be obtained under the conditions here investigated. On the other hand, Ni-Phyllosilicate and Zn-Phlogopite are good candidates to incorporate organic guest in their interlayered spaces. Thus, aminopropyl-modified Ni-Phyllosilicates and Zn-Phlogopites were prepared using TEOS and APTS as silica sources in different ratios (5, 10, 25 and 50% of APTS) and were obtained with good crystallinity. In a second set of experiment, the aminopropyl-modified minerals were prepared in the presence of PBA and the inorganic phases were obtained satisfactory. However, the presence of imide modes could not be observed by the techniques employed. Fluorescence results show that the presence of PBA change the materials' interaction with light. Particularly, aminopropyl-modified PBI@Zn-phlogopite (10% APTS) shows the highest emission, at 484 nm.

SANTRAUKA

VILNIAUS UNIVERSITETAS CHEMIJOS IR GEOMOKSLŲ FAKULTETAS

RŪTA GERULAITYTĖ

PERYLENO DAŽAI NATŪRALIAI FLUORESCUOJANČIUOSE MINERALUOSE: HIBRIDINIŲ MEDŽIAGŲ SINTEZĖ HIDROTERMIU METODU

Buvo paruošti ir modifikuoti keturi fluorescenciniai mineralai iš filosilikatų šeimos ir modifikuoti organiniais chromoforais, siekiant pakeisti jų fluorescencinį elgesį. Mineralų kristalizacijos metu hidroterminės sintezės metu bandyta įterpti organinį perileno-3,4,9,10-tetrakarboksilo dianhidridą (PBA). Visi mineralai ir jų atitinkami hibridai buvo ištirti SEM, PXRD, ATR-FTIR, UV-Vis ir fluorescencijos spektroskopija. Gyrolitas ir Ni-Hektoritai į savo struktūras neleidžia įterpti organinių grupių. Kaip rodo XRD, kristalinės struktūros negali būti gautos tiriamomis sąlygomis. Kita vertus, Ni-filosilikatai ir Zn-Phlogopitas yra geri kandidatai įtraukti organinius junginius į savo tarpfluoksnis. Taigi, aminopropilo modifikuoti nikelio filosilikatai ir Zn-Phlogopitai buvo paruošti naudojant TEOS ir APTS kaip silicio dioksido šaltiniai skirtingais santykiais (5, 10, 25 ir 50% APTS) ir buvo gauti geri kristališkumai. Antroje eksperimento dalyje aminopropilu modifikuoti mineralai buvo apdoroti PBA dažu ir gautos patenkinamos neorganinės fazės. Tačiau imido režimo buvimo nebuvo galima identifikuoti naudojant taikomus metodus. Fluorescencijos rezultatai rodo, kad PBA buvimas gali pakeisti medžiagų sąveiką su šviesa. Ypač aminopropilu modifikuotas PBI @ Zn-phlogopite (10% APTS) skleidžia didžiausią emisiją, esant 484 nm.

ACKNOWLEDGEMENTS

I would like to acknowledge Professor Aivaras Kareiva and Professor Miriam M. Unterlass from Technische Universität Wien for inspiring my interest in the development of innovative technologies.

I would like to thank Doctor Živilė Stankevičiūtė for all the help during master thesis work.